

# MANIFOLD APPROXIMATIONS VIA TRANSPORTED SUBSPACES: MODEL REDUCTION FOR TRANSPORT-DOMINATED PROBLEMS

DONSUB RIM\*, BENJAMIN PEHERSTORFER\*, AND KYLE T. MANDLI†

**Abstract.** This work presents a method for constructing online-efficient reduced models of large-scale systems governed by parametrized nonlinear scalar conservation laws. The solution manifolds induced by transported-dominated problems such as hyperbolic conservation laws typically exhibit nonlinear structures, which means that traditional model reduction methods based on linear approximations are inefficient when applied to these problems. In contrast, the approach introduced in this work derives reduced approximations that are nonlinear by explicitly composing global transport dynamics with locally linear approximations of the solution manifolds. A time-stepping scheme evolves the nonlinear reduced models by transporting local approximation spaces along the characteristic curves of the governing equations. The proposed computational procedure allows an offline/online decomposition and is online efficient in the sense that the costs of time-stepping the nonlinear reduced models are independent of the number of degrees of freedom of the full model. Numerical experiments with transport through heterogeneous media and the Burgers' equation show orders of magnitude speedups of the proposed nonlinear reduced models based on transported subspaces compared to traditional linear reduced models and full models.

**Key words.** Model reduction, transport-dominated problems, nonlinear approximations, transported subspaces

**AMS subject classifications.** 78M34, 41A46, 35F20, 78M12

**1. Introduction.** Model reduction for transport-dominated problems can be challenging because the corresponding solution manifolds typically exhibit high dimensional features and so can only be well-approximated by subspaces if their dimension is high; that is, the Kolmogorov  $N$ -widths of the solution manifolds decay slowly [15, 6]. To overcome this challenge of slowly decaying Kolmogorov  $N$ -widths, this work introduces transported subspaces, which are subspaces conjoined with nonlinear transportation. The corresponding approximation is nonlinear and so can lead to efficient reduced models even if the Kolmogorov  $N$ -widths of the solution manifolds decay slowly.

The difficulty in developing reduced models for transport-dominated problems was recognized in [26], which also introduced a template-fitting approach. Subsequent works to overcome this problem fall broadly into two groups. The first group attempts to find relevant nonlinear transformations of the solution manifolds. The method of freezing based on the Lax-Pair decomposition of the differential operator was devised in [14]. The work [8] made a connection to the optimal transport problem in finding a nonlinear low-dimensional structure. More works in this group include shock curve estimation [30], shifted proper orthogonal decomposition (sPOD) [20], greedy generalization of template-fitting [25], transformed snapshot interpolation [36, 37], a machine-learning approach based on autoencoders [10], characteristic dynamic mode decomposition [28], registration methods [29], Wasserstein barycenters [33], and offline pre-processing by invertible maps [13]. For nonlinear hyperbolic conservation laws [12], there is a relationship between optimal transport and scalar conservation laws [3], and it was demonstrated in [23, 24] that a nonlinear interpolation procedure called displacement interpolation by pieces (DIP) is able to capture

---

\*Courant Institute of Mathematical Sciences, New York University, New York, NY 10012 ([dr1653@nyu.edu](mailto:dr1653@nyu.edu), [pehersto@cims.nyu.edu](mailto:pehersto@cims.nyu.edu)).

†Department of Applied Physics and Applied Mathematics, Columbia University, New York, NY 10027 ([kyle.mandli@columbia.edu](mailto:kyle.mandli@columbia.edu)).

the nonlinear transport structure, which leads to localized reduced models.

The second group focuses on online adaptive methods that update local reduced spaces depending on time and parameters. For example, the work [4] proposes an adaptive refinement of reduced bases similar to  $h$ -adaptive finite-element approaches. In [18, 17], the locality of coherent structures that are transported through the spatial domain is exploited to adapt spaces from only a few samples. While these adaptive procedures achieve speedups compared to traditional reduced models, the corresponding computational methods have costs that scale with the complexity of the full-model discretization. Additional works that examine related aspects of transported-dominated problems include the use of  $L^1$ -norm minimization [1] and the Petrov-Galerkin space-time approach [38].

The model reduction method proposed in this work is called Manifold Approximations via Transported Subspaces (MATS) and merges ideas from both groups mentioned above. MATS produces an adaptive scheme that uses nonlinear transformations to generate an adaptive reduced basis during the online stage. Although the effect of the transformation is nonlinear, the transformation itself is built from a linear combination of low-rank transport modes. This specific structure enables the derivation of the time-dependent adaptation directly from the governing equations. Combining the MATS procedure with a projection-based time update results in online-efficient reduced models.

Three main ideas are introduced in this work:

- (1) the transported subspace generated by low-rank transport modes that are explicit to derive and compute, which provide a low-rank approximation to the transport dynamics necessary to approximate the solution manifold,
- (2) interpolation particles that enable online-efficient adaptations of transported subspaces,
- (3) an online-efficient time-stepping scheme for the proposed reduced model.

This manuscript is organized as follows. In section 2, we formulate our problem setup and set forth basic notations. In section 3, we introduce a notion of a Kolmogorov width for transported subspaces. In section 4, we provide a concrete procedure for constructing the transported subspaces. In section 5, we construct the reduced model by building on the notion of interpolation particles and the change of basis formula. An algorithmic summary is given in section 6. In section 7, we provide numerical examples that illustrate the speedups obtained with our method.

**2. Problem formulation and preliminaries.** In this section, we describe the parametrized partial differential equations (PDE) under consideration and introduce notations and definitions to be used throughout the work.

**2.1. Parametrized scalar conservation laws.** For the spatial domain  $\Omega := (x_\ell, x_r) \subset \mathbb{R}$  with  $|x_\ell|, |x_r| < \infty$ , and for parameters  $\boldsymbol{\mu} \in \mathcal{D} \subset \mathbb{R}^d$ , we seek a solution  $u \in C^1(\Omega \times (0, t_F) \times \mathcal{D})$  that maps into  $\mathbb{R}$  and satisfies

$$(2.1) \quad \begin{cases} \partial_t u + \partial_x [f(u, x; \boldsymbol{\mu})] = \psi(u, x; \boldsymbol{\mu}), & (x, t) \in \Omega \times (0, t_F), \\ u(x, 0) = u_0(x), \\ u(x_\ell, t) = u_0(x_\ell), \end{cases}$$

in which  $f(\cdot, \cdot; \boldsymbol{\mu}) \in C^\infty(\mathbb{R}^2)$  is a convex function in the first variable and  $\psi(\cdot, \cdot; \boldsymbol{\mu}) \in C^\infty(\mathbb{R}^2)$ . The initial condition  $u_0(x)$  and the boundary condition  $u(x_\ell, t)$  are independent of time and parameter. For a fixed parameter  $\boldsymbol{\mu}$ , the initial boundary value problem (2.1) has been studied analytically and numerically [9, 27, 12].

**2.2. Reduced approximation.** Let us denote the time-parameter domain by  $\mathcal{H} := (0, t_F) \times \mathcal{D}$ . For all  $(t, \boldsymbol{\mu}) \in \mathcal{H}$ , the solution  $u(\cdot, t; \boldsymbol{\mu})$  of (2.1) is in the space  $\mathbb{V} := C^0(\Omega)$  equipped with the inner product  $(f, g) := \int_{\Omega} fg \, dx$  for  $f, g \in \mathbb{V}$ . The inner product induces the norm  $\|\cdot\|_{\mathbb{V}}$ . Let us denote by  $u_{\delta} \in C^0(\Omega \times (0, t_F) \times \mathcal{D})$  a continuous piecewise polynomial approximation of  $u$ , to which we refer to as the full-model solution in the following. Let  $\mathbb{V}_{\delta} \subset \mathbb{V}$  be the space of continuous piecewise polynomial functions defined on a grid  $x_{\ell} < x_{\ell} + \Delta x < \dots < x_{\ell} + (N_{\delta} - 1)(\Delta x) = x_r$  of uniform width  $\Delta x = \delta$  (that is,  $(N_{\delta} - 1)\delta = |\Omega|$ ). Let  $\{\varphi_n\}_{n=1}^{N_{\delta}}$  be a basis of  $\mathbb{V}_{\delta}$ , then suppose we can represent  $u_{\delta}$  as a linear combination of this basis,

$$(2.2) \quad u_{\delta}(x; t, \boldsymbol{\mu}) = \sum_{n=1}^{N_{\delta}} b_n(t, \boldsymbol{\mu}) \varphi_n(x),$$

for coefficients  $\{b_n(t, \boldsymbol{\mu})\}_{n=1}^{N_{\delta}}$ . We assume that the  $u_{\delta}$  is a uniformly accurate approximation to the classical solution  $u$ , i.e., there exists a constant  $C > 0$  such that for all  $(t, \boldsymbol{\mu}) \in \mathcal{H}$ , the bound

$$(2.3) \quad \|u(\cdot, t; \boldsymbol{\mu}) - u_{\delta}(\cdot, t; \boldsymbol{\mu})\|_{\mathbb{V}} \leq C\delta^r$$

holds for some  $r \geq 1$ . The solution manifold  $\mathcal{M}_{\delta}$  corresponding to the full-model solutions of (2.1) is

$$(2.4) \quad \mathcal{M}_{\delta} := \{u_{\delta}(\cdot, t; \boldsymbol{\mu}) : (t, \boldsymbol{\mu}) \in \mathcal{H}\} \subset \mathbb{V}_{\delta}.$$

The Kolmogorov  $N$ -width [19] of the solution manifold  $\mathcal{M}_{\delta}$  is

$$(2.5) \quad d(N; \mathcal{M}_{\delta}) = \inf_{\substack{\mathbb{V}_{\text{rb}} \subset \mathbb{V} \\ \dim(\mathbb{V}_{\text{rb}}) = N}} \sup_{u_{\delta} \in \mathcal{M}_{\delta}} \inf_{v \in \mathbb{V}_{\text{rb}}} \|u_{\delta} - v\|_{\mathbb{V}},$$

and gives the best possible error of approximating functions in  $\mathcal{M}_{\delta}$  in a subspace  $\mathbb{V}_{\text{rb}} \subset \mathbb{V}_{\delta}$  of dimension  $N = \dim \mathbb{V}_{\text{rb}}$ . Traditional model reduction aims to construct a basis  $\{\zeta_n\}_{n=1}^N$  of a subspace  $\mathbb{V}_{\text{rb}} \subset \mathbb{V}_{\delta}$  in which the solution in  $\mathcal{M}_{\delta}$  can be approximated well. The reduced approximation is a linear combination of the basis  $\{\zeta_n\}_{n=1}^N$ ,

$$(2.6) \quad u_{\text{rb}}(x; t, \boldsymbol{\mu}) = \sum_{n=1}^N \beta_n(t, \boldsymbol{\mu}) \zeta_n(x),$$

with coefficients  $\{\beta_n(t, \boldsymbol{\mu})\}_{n=1}^N$ ; see, e.g., [7, 16] and references therein.

For problems of hyperbolic or transport-dominated types, the Kolmogorov  $N$ -width of  $\mathcal{M}_{\delta}$  for the problem (2.1) can decay slowly [14, 6], which implies that traditional model reduction fails: to obtain an acceptable accuracy with a reduced approximation of the form (2.6), the number of terms  $N$ , and thus the dimension of  $\mathbb{V}_{\text{rb}}$ , must be large.

**3. Transported subspaces.** To overcome the limitation of reduced approximations of the form (2.6), we introduce approximations that adaptively vary the subspace  $\mathbb{V}_{\text{rb}}$  by using a different subspace  $\mathbb{V}_{\text{rb}}(t, \boldsymbol{\mu})$  depending on  $(t, \boldsymbol{\mu}) \in \mathcal{H}$ . This section proposes a specific structure for constructing these adaptive subspaces. It builds on what we will call low-rank transport maps, which lead to subspaces of low dimension and, at the same time, guarantee straightforward basis adaptations with respect to time and parameters.

Furthermore, we provide an intuition as to why our construction is expected to produce an accurate approximation for solution manifolds of transport-dominated problems. We do so by providing a generalization of the notion of the Kolmogorov  $N$ -width (2.5), which we call the  $(N, M)$ -width. The new argument  $M$  corresponds to the dimension of the space of low-rank transport maps. We give examples of transport-dominated problems for which the  $(N, M)$ -width decays rapidly and the Kolmogorov  $N$ -width decays slowly.

**3.1. Low-rank space of transport maps.** We develop the notion of the *low-rank space of transport maps* which is a subset of certain diffeomorphisms. We aim to form a space containing transformations of the domain, but directly using diffeomorphisms of the finite open interval  $\Omega = (x_\ell, x_r)$  encounters a technical issue, that it is not closed under addition, i.e., adding two such diffeomorphisms does not produce a map whose range is in  $\Omega$  in general. To allow function space operations (additions and scalar multiplications) we define spaces of transport maps on the entire real line.

**DEFINITION 3.1.** *Let  $\mathbb{T}$  denote the subgroup of diffeomorphisms on  $\mathbb{R}$  that are increasing (strictly monotone).*

Function compositions (pullbacks) will play a key role. We will denote by  $\flat$  the composition of  $\xi : \mathbb{R} \rightarrow \mathbb{R}$  with the inverse of  $T \in \mathbb{T}$ ,

$$(3.1) \quad T^\flat \xi(x) := \xi(T^{-1}(x)).$$

Next we define the composition with the functions defined on the domain  $\Omega$  by extending them to the real line.

**DEFINITION 3.2.** *Let  $T \in \mathbb{T}$  and let  $\xi : \Omega \rightarrow \mathbb{R}$  be continuous. Let  $\bar{\xi}$  be defined from  $\xi$  by*

$$(3.2) \quad \bar{\xi}(x) := \begin{cases} \xi(x_\ell) & \text{if } x \leq x_\ell, \\ \xi(x) & \text{if } x_\ell < x < x_r, \\ \xi(x_r) & \text{if } x_r \leq x. \end{cases}$$

*Then, we define  $T^\flat \xi : \Omega \rightarrow \mathbb{R}$  by  $T^\flat \xi(x) := T^\flat \bar{\xi}(x)$ .*

Let us construct a map  $\hat{T}$  from the linear combination of given linearly independent functions  $\{v_m\}_{m=1}^M \subset \mathbb{T}$ ,

$$(3.3) \quad \hat{T}(x) := \sum_{m=1}^M \alpha_m v_m(x).$$

In general it does not hold that  $\hat{T} \in \mathbb{T}$ , since  $\mathbb{T}$  is not a function space. Nonetheless, we will focus on  $\hat{T} \in \text{span}\{v_m\}_{m=1}^M$  that also satisfy  $\hat{T} \in \mathbb{T}$ , arriving at the next definition.

**DEFINITION 3.3.** *Given linearly independent  $\{v_m\}_{m=1}^M \subset \mathbb{T}$ ,  $\mathbb{S} \subset \mathbb{T}$  is a finite-dimensional subspace of  $\mathbb{T}$ , denoted by  $\mathbb{S} \subset \mathbb{T}$ , if*

$$(3.4) \quad \mathbb{S} = \mathbb{T} \cap \text{span}\{v_m\}_{m=1}^M.$$

*We will refer to  $\{v_m\}_{m=1}^M$  as the basis of  $\mathbb{S}$ , and let  $\dim(\mathbb{S}) := M$ .*

Note that by construction, we required that  $\hat{T} \in \mathbb{S} \subset \mathbb{T}$  be increasing, i.e., that  $x_1 < x_2$  implies  $\hat{T}(x_1) < \hat{T}(x_2)$ . But more generally,  $\hat{T} \in \text{span}\{v_m\}_{m=1}^M$  with arbitrary

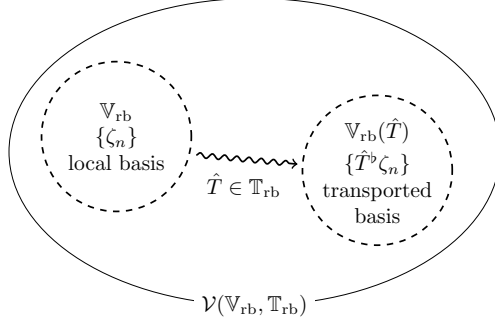


FIG. 3.1. Diagram depicting the local and global approximations using  $\mathcal{V}(\mathbb{V}_{rb}, \mathbb{T}_{rb})$ , which is generated by transporting the subspace  $\mathbb{V}_{rb}$  using  $\hat{T} \in \mathbb{T}_{rb}$ .

coefficients  $\{\alpha_m\}_{m=1}^M$  in (3.3) is not necessarily increasing. The consequence is that the inverse of  $\hat{T}$  becomes ill-defined. A sufficient condition for  $\hat{T} \in \mathbb{T}$  is that  $\hat{T}' > 0$ , which results in a set of constraints on its coefficients  $\{\alpha_m\}_{m=1}^M$ . Hence, certain additions and scalar multiplications are allowed within  $\mathbb{S} \subset \mathbb{T}$ , e.g. within a neighborhood of the identity  $\text{Id} \in \mathbb{T}$ , but  $\mathbb{S}$  is not closed under these function space operations.

**3.2. The Kolmogorov  $(N, M)$ -width.** We consider the nonlinear generalization of the reduced approximation (2.6) in which the basis functions  $\{\zeta_n\}_{n=1}^N$  of  $\mathbb{V}_{rb}$  are composed with the inverse of  $T \in \mathbb{T}$ . That is, we consider approximating elements of the solution manifold  $\mathcal{M}_\delta$  by functions lying in the collection  $\mathcal{V}$  defined by

$$(3.5) \quad \mathcal{V}(\mathbb{V}_{rb}, \mathbb{T}) := \bigcup_{T \in \mathbb{T}} \mathbb{V}_{rb}(T), \quad \mathbb{V}_{rb}(T) := \{T^b \xi : \xi \in \mathbb{V}_{rb}\}.$$

In particular, we can restrict  $\mathcal{V}$  to use transport maps in  $\mathbb{T}_{rb} \subset \mathbb{T}$  (Definition 3.3), resulting in the collection  $\mathcal{V}(\mathbb{V}_{rb}, \mathbb{T}_{rb})$ .

Now we extend the notion of the Kolmogorov  $N$ -width (2.5) to describe the effectiveness of the collection  $\mathcal{V}(\mathbb{V}_{rb}, \mathbb{T}_{rb})$  in approximating the solution manifold  $\mathcal{M}_\delta$ .

DEFINITION 3.4. Define the Kolmogorov  $(N, M)$ -width as

$$(3.6) \quad d(N, M; \mathcal{M}_\delta) = \inf_{\substack{\mathbb{V}_{rb} \subset \mathbb{V} \\ \dim(\mathbb{V})=N \\ \mathbb{T}_{rb} \subset \mathbb{T} \\ \dim(\mathbb{T}_{rb})=M}} \sup_{u_\delta \in \mathcal{M}_\delta} \inf_{v \in \mathcal{V}(\mathbb{V}_{rb}, \mathbb{T}_{rb})} \|u_\delta - v\|_{\mathbb{V}}.$$

It is immediate that

$$(3.7) \quad d(N; \mathcal{M}_\delta) = d(N, 1; \mathcal{M}_\delta), \quad d(N; \mathcal{M}_\delta) \geq d(N, M; \mathcal{M}_\delta) \text{ for all } M \in \mathbb{N}.$$

Intuitively speaking, the low-rank basis  $\{\zeta_n\}_{n=1}^N$  of  $\mathbb{V}_{rb}$  spans the *local* linearization of the solution manifold; whereas the *global* transport-dominated behavior of the solution is approximated by the basis  $\{v_m\}_{m=1}^M$  of  $\mathbb{T}_{rb}$ . This overall strategy is illustrated as a diagram in Figure 3.1.

Note that this  $(N, M)$ -width is related to the nonlinear Kolmogorov width introduced in [31], where multiple subspaces with identical dimension are used in the approximation of  $\mathcal{M}_\delta$ . However, the nonlinear Kolmogorov width of  $\mathcal{V}(\mathbb{V}_{rb}, \mathbb{T}_{rb})$  can be large in general, even when the dimensions of  $\mathbb{V}_{rb}$  and  $\mathbb{T}_{rb}$  are small.

For systems of conservation laws, the scalar problem (2.1) is extended into multiple state variables: the solution  $u$  takes on vector values and the flux function  $f(\cdot, x; \boldsymbol{\mu})$  satisfies a generalized convexity condition [12]. In this case, each state variable is a superposition of time-dependent characteristic variables, each with a corresponding set of characteristic curves. As a result, the approximations in  $\mathcal{V}(\mathbb{V}_{\text{rb}}, \mathbb{T}_{\text{rb}})$ , as well as the corresponding notion of  $(N, M)$ -width, is no longer sufficient. But a straightforward extension is possible by a superposition.

DEFINITION 3.5. The Kolmogorov  $(N, M, L)$ -width is given by

$$(3.8) \quad d(N, M, L; \mathcal{M}_\delta) = \inf_{\substack{\mathbb{V}_{\text{rb}} \subset \mathbb{V} \\ \dim(\mathbb{V}_{\text{rb}}) = N \\ \mathbb{T}_{\text{rb}} \subset \mathbb{T} \\ \dim(\mathbb{T}_{\text{rb}}) = M}} \sup_{u_\delta \in \mathcal{M}_\delta} \inf_{v_\ell \in \mathcal{V}(\mathbb{V}_{\text{rb}}, \mathbb{T}_{\text{rb}})} \left\| u_\delta - \sum_{\ell=1}^L v_\ell \right\|_{\mathbb{V}}.$$

Again,  $d(N, M, 1; \mathcal{M}_\delta) = d(N, M; \mathcal{M}_\delta)$ ,  $d(N, M; \mathcal{M}_\delta) \geq d(N, M, L; \mathcal{M}_\delta)$ . Various extensions to multiple spatial dimensions are possible, for example by letting the transport map to be a diffeomorphism in higher dimensions [29]. For hyperbolic problems in particular, one can use the Radon transform [22, 21].

**3.3. Decay of Kolmogorov  $(N, M)$ -width.** For intuition, we briefly discuss the decay of the  $(N, M)$ -width with examples.

*Example 3.6* (Linear advection). Consider a 1-parameter linear advection problem  $f(u; \boldsymbol{\mu}_1) = \mu_1 u$ ,  $\psi = 0$  and  $u_0(x) = \phi(x)$ , for which  $(t, \boldsymbol{\mu}) = (t, \mu_1)$ . The solution manifold has a small  $(N, M)$ -width, which can be seen by letting  $\mathbb{V}_{\text{rb}} := \text{span}\{\phi(x)\}$  and  $\mathbb{T}_{\text{rb}} = \text{span}\{1, x\}$ . Then  $d(1, 2; \mathcal{M}_\delta) = \mathcal{O}(\delta^r)$ , achieving an error at the level of the full-model discretization error (2.3).

*Example 3.7* (Gibbs phenomenon). If we further restrict  $\mathbb{V}_{\text{rb}}$  in (2.5) and (3.6) to be a subset of the Chebyshev basis of dimension  $N$  and define the corresponding  $N$ - and  $(N, M)$ -width as  $\tilde{d}(N; \mathcal{M}_\delta)$  and  $\tilde{d}(N, M; \mathcal{M}_\delta)$ , it is known that for a solution manifold containing the signum function  $\text{sign} : [-1, 1] \rightarrow \{-1, 0, 1\}$  with a jump at  $x = 0$ , it holds that  $\tilde{d}(N; \mathcal{M}_\delta) \geq c/N$  for some  $c > 0$ ; see [32]. However, allowing the diffeomorphism  $\mathbb{T}_{\text{rb}} = \{x^{2q+1}\}$  with large enough  $q \in \mathbb{N}$  to transform  $\mathbb{V}_{\text{rb}} = \{x\}$  has the consequence that  $\tilde{d}(1, 1; \mathcal{M}_\delta) = \mathcal{O}(\delta)$ .

*Example 3.8* (Burgers turbulence). One can show that a continuous piecewise linear discretization of white noise, in the form of (2.2) with  $\{\varphi_n\}$  nodal basis functions and independent coefficients  $\{b_n\}$  drawn from normal distributions, does not have a small  $(N, M)$ -width for small  $N$  and  $M$ . Considering the solution to the Burgers equation with such a random initial condition, it can be shown that the solution manifold for this problem has a large  $(N, M)$ -width during a time interval  $[0, \varepsilon)$  for which  $\varepsilon$  is small enough.

*Example 3.9* (Wave equation). The wave equation  $\partial_{tt}u + \partial_{xx}u = 0$  can propagate waves in two opposite directions, and can be written in a first order system of the type (2.1) with two variables (see e.g. [12]). As discussed above, in this case  $d(N, 2; \mathcal{M}_\delta)$  can decay slowly with respect to  $N$  since one transport map cannot represent in a low-rank manner a superposition of two waves traveling at different speeds when the two waves intersect. However, one can show  $d(N, 2, 2; \mathcal{M}_\delta) = \mathcal{O}(\delta^r)$ .

**3.4. Reduced nonlinear approximation.** In the Kolmogorov  $(N, M)$ -width, it is implicit that there exist for each  $u_\delta \in \mathcal{M}_\delta$  an approximation  $v \in \mathcal{V}(\mathbb{V}_{\text{rb}}, \mathbb{T}_{\text{rb}})$

that minimizes the error  $\|u_\delta - v\|_{\mathbb{V}}$ . Thus, a fast decay in the  $(N, M)$ -width is only a non-constructive statement. In later sections, we propose a constructive method that finds an approximation in  $\mathcal{V}(\mathbb{V}_{\text{rb}}, \mathbb{T}_{\text{rb}})$ . Given  $u_\delta(\cdot, t; \boldsymbol{\mu}) \in \mathcal{M}_\delta$ , the method provides an algorithm for computing the reduced approximation  $\hat{u}(\cdot, t; \boldsymbol{\mu}) \in \mathcal{V}(\mathbb{V}_{\text{rb}}, \mathbb{T}_{\text{rb}})$ . Then, for each fixed  $(t, \boldsymbol{\mu}) \in \mathcal{H}$ ,  $\hat{u}$  can be expressed as

$$(3.9) \quad \begin{cases} \hat{u}(x, t; \boldsymbol{\mu}) = \sum_{n=1}^N \beta_n(t, \boldsymbol{\mu}) \hat{T}_{(t, \boldsymbol{\mu})}^{\flat} \zeta_n(x), \\ \hat{T}_{(t, \boldsymbol{\mu})}(x) = \sum_{m=1}^M \alpha_m(t, \boldsymbol{\mu}) v_m(x). \end{cases}$$

The reduced approximation  $\hat{u}(\cdot, t; \boldsymbol{\mu})$  is described by two sets of coefficients: the transport coefficients  $\{\alpha_m(t, \boldsymbol{\mu})\}_{m=1}^M$  and the local basis coefficients  $\{\beta_n(t, \boldsymbol{\mu})\}_{n=1}^N$ . The reduced approximation (3.9) relies on a different reduced subspace  $\mathbb{V}_{\text{rb}}(\hat{T}_{(t, \boldsymbol{\mu})})$  for different  $(t, \boldsymbol{\mu}) \in \mathcal{H}$ . We call this subspace corresponding to  $(t, \boldsymbol{\mu})$  a *transported subspace* as described in the following definition.

**DEFINITION 3.10.** *Let us denote by  $\hat{T}_{(t, \boldsymbol{\mu})} \in \mathbb{T}_{\text{rb}} \subset \mathbb{T}$  a transport map corresponding to  $(t, \boldsymbol{\mu}) \in \mathcal{H}$ . The transported subspace is a space generated by compositions of functions in the space  $\mathbb{V}_{\text{rb}}$  with the inverse of  $\hat{T}_{(t, \boldsymbol{\mu})}$ ,*

$$(3.10) \quad \mathbb{V}_{\text{rb}}(t, \boldsymbol{\mu}) := \mathbb{V}_{\text{rb}}(\hat{T}_{(t, \boldsymbol{\mu})}) = \{\hat{T}_{(t, \boldsymbol{\mu})}^{\flat} \xi : \xi \in \mathbb{V}_{\text{rb}}\}, \quad (t, \boldsymbol{\mu}) \in \mathcal{H}.$$

Note that  $\mathbb{V}_{\text{rb}}(t, \boldsymbol{\mu}) \not\subset \mathbb{V}_\delta$  in general, so the transported subspaces are not necessarily conforming with respect to the full-model space  $\mathbb{V}_\delta$ .

**4. Offline construction of low-rank transport space.** In this section, we discuss a procedure that constructs the bases  $\{v_m\}_{m=1}^M$  of  $\mathbb{T}_{\text{rb}}$  and  $\{\zeta_n\}_{n=1}^N$  of  $\mathbb{V}_{\text{rb}}$  to be used in the nonlinear reduced approximation (3.9). A key feature of our procedure is that it relies only on well-understood linear dimensionality reduction techniques such as the singular value decomposition (SVD), rather than requiring the solution of special, potentially non-convex, optimization problems.

We first recall definitions related to a nonlinear interpolation procedure called displacement interpolation by pieces (DIP) introduced in [23, 24]. The interpolation proceeds by decomposing  $u_\delta(\cdot, t; \boldsymbol{\mu})$  into a sum of monotone functions, then computing the optimal transport map between the corresponding monotone functions. One combines these maps to obtain the DIP maps, a collection of transport maps in  $\mathbb{T}$ . By constructing a low-rank approximation to the so-called DIP maps, we obtain the basis  $\{v_m\}_{m=1}^M$  to be used in the nonlinear reduced approximation (3.9). We then discuss the construction of the basis  $\{\zeta_n\}_{n=1}^N$ .

*Remark 4.1.* From here and onwards, we will assume that the full model is first order accurate ( $r = 1$  in (2.3)), since a finite volume method (FVM) with Godunov flux is total variation diminishing (TVD) without requiring additional modifications, e.g. limiters or non-oscillatory higher-order reconstructions. As a result, the full model as well as the corresponding estimate (2.3) extends to the non-classical solutions of (2.1) without changes (see [12]). Therefore, this choice simplifies our exposition without limiting the extensibility to the non-classical case. We take as  $u_\delta$  the continuous piecewise-linear reconstruction of such a FVM solution in the form (2.2). The constructive methods proposed in this and subsequent sections can be extended to the higher-order case ( $r > 1$ ) with more work.

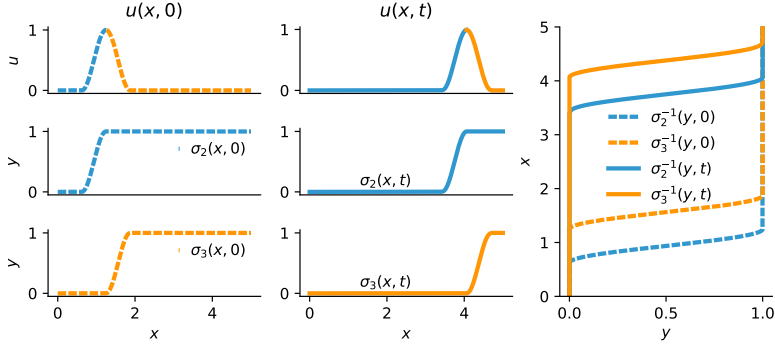


FIG. 4.1. The monotone decomposition (4.1) for the solution  $u(x, t)$  to the advection equation for two different times (left) with  $\gamma_2 = 1, \gamma_3 = -1$ . The inverse of  $\sigma_2, \sigma_3$  (right).

**4.1. Monotone decomposition.** In order to define DIP, we first define the *monotone decomposition* which decomposes the solution into a sum of monotone functions. We start by making a preliminary statement that the continuous piecewise-linear  $u_\delta(\cdot, t; \boldsymbol{\mu})$  can be decomposed as a sum of certain non-decreasing functions.

LEMMA 4.2. *One can represent  $u_\delta(\cdot, t; \boldsymbol{\mu}) \in \mathcal{M}_\delta$  (2.2) as a sum*

$$(4.1) \quad u_\delta(x, t; \boldsymbol{\mu}) = u_\delta(x_*, t; \boldsymbol{\mu}) + \sum_{j=1}^J \gamma_j(t, \boldsymbol{\mu}) \sigma_j(x, t; \boldsymbol{\mu}),$$

where  $x_* \in \Omega$  is a fixed point,  $\gamma_j \in \mathbb{R}$ , and the functions  $\sigma_j(\cdot, t; \boldsymbol{\mu}) : \Omega \rightarrow [0, 1]$  satisfy:

- (i)  $\sigma_j$  is continuous, piecewise linear, and non-decreasing,
- (ii)  $\sigma_j(x_\ell) = 0$  and  $\sigma_j(x_r) = 1$ ,
- (iii) strictly increasing in  $\sigma_j^{-1}((0, 1))$ ,
- (iv)  $\text{int}(\text{supp } \sigma'_j) \cap \text{int}(\text{supp } \sigma'_k) = \emptyset$  if  $j \neq k$  where  $\text{int}(\cdot)$  is the interior of a set,
- (v)  $j < k$  implies  $\text{supp } \sigma'_j \leq \text{supp } \sigma'_k$ ,
- (vi)  $\Omega = \cup_{j=1}^J \text{supp } \sigma'_j$ .

*Proof.* Recall the expression for  $u_\delta(x, t; \boldsymbol{\mu})$  (2.2), where we let  $\varphi_n(x)$  be the hat function, i.e. continuous piecewise linear function such that  $\varphi_n(x_\ell + (m-1)\Delta x) = \delta_{n,m}$  where  $\delta_{n,m}$  is the Kronecker delta and  $n, m = 1, \dots, N_\delta$ . Now, let  $\varsigma_n := \sum_{m=n}^{N_\delta} \varphi_m$  then

$$(4.2) \quad u_\delta(x, t; \boldsymbol{\mu}) = \sum_{n=1}^{N_\delta} \beta_n(t, \boldsymbol{\mu}) \varphi_n(x) = \beta_1 \varsigma_1(x) + \sum_{n=2}^{N_\delta} (\beta_n(t, \boldsymbol{\mu}) - \beta_{n-1}(t, \boldsymbol{\mu})) \varsigma_n(x),$$

so that letting  $x_* := x_\ell$ ,  $J := N_\delta - 1$ ,  $\sigma_j := \varsigma_{j+1}$ ,  $\gamma_j := \beta_{j+1} - \beta_j$ ,

$$(4.3) \quad u(x, t; \boldsymbol{\mu}) = u(x_*, t; \boldsymbol{\mu}) + \sum_{j=1}^J \gamma_j(t, \boldsymbol{\mu}) \sigma_j(x).$$

Note that  $\sigma_j$  is continuous, piecewise linear, non-increasing function,  $\sigma_j(x_\ell) = 0$ ,  $\sigma_j(x_r) = 1$ , and  $\text{supp } \sigma'_j = [x_\ell + (j-1)\Delta x, x_\ell + j\Delta x]$  with  $\sigma_j^{-1}((0, 1)) = \text{int}(\text{supp } \sigma'_j)$  in which it is strictly increasing with  $\sigma'_j = 1/\Delta x$ .  $\square$

DEFINITION 4.3. *A monotone decomposition of  $u_\delta(\cdot, t; \boldsymbol{\mu}) \in \mathcal{M}_\delta$  is the sum (4.1) with the minimal  $J \in \mathbb{N}$ .*



For an illustration of the monotone decomposition of solutions to the advection equation, see [Figure 4.1](#). Since  $u_\delta$  is continuous and piecewise linear in our setting, an exact decomposition [\(4.1\)](#) is available. In more general settings, the identity in [\(4.1\)](#) can be relaxed to an approximation.

Note that one can extrapolate  $\sigma_j(\cdot, t; \boldsymbol{\mu})$  defined in the bounded domain  $\Omega = (x_\ell, x_r)$  to the real line  $\mathbb{R}$ , by letting  $\sigma_j(x, t; \boldsymbol{\mu})$  be 0 if  $x \leq x_\ell$  and 1 if  $x \geq x_r$ . This extends  $u_\delta(\cdot; t, \boldsymbol{\mu})$  also to the real line (equivalent to [\(3.2\)](#)). Also note that since the full model is assumed to be TVD, the corresponding  $u_\delta$  for the homogeneous version of [\(2.1\)](#) has  $J$  decreasing over time.

**4.2. Signature condition and DIP maps.** We introduce the signature condition which is relevant when comparing the decomposition [\(4.1\)](#) for  $u_\delta(\cdot, t; \boldsymbol{\mu}) \in \mathcal{M}_\delta$  across different values of  $(t, \boldsymbol{\mu}) \in \mathcal{H}$ . Let us collect snapshots of  $u_\delta(\cdot, t; \boldsymbol{\mu})$  at various values of  $(t, \boldsymbol{\mu}) \in \mathcal{H}_g$  designated by the set

$$(4.4) \quad \mathcal{H}_g := \{(t_1, \boldsymbol{\mu}_1), (t_2, \boldsymbol{\mu}_2), \dots, (t_{N_g}, \boldsymbol{\mu}_{N_g})\}.$$

Then, we denote the collection of snapshots of  $u_\delta$  by

$$(4.5) \quad \mathcal{S}_g := \{u_\delta(\cdot, t; \boldsymbol{\mu}) : (t, \boldsymbol{\mu}) \in \mathcal{H}_g\}.$$

Now, we define the signature condition on  $\mathcal{S}_g$ .

**DEFINITION 4.4** (Signature condition). *A set of snapshots  $\mathcal{S}_g$  [\(4.5\)](#) satisfies the signature condition if each snapshot in the set has a monotone decomposition ([Definition 4.3](#), [\(4.1\)](#)) that holds with the same  $x_* \in \Omega$  and vector  $(\text{sign}(\gamma_j))_{j=1}^J$ .*

If  $\mathcal{S}_g$  satisfies the signature condition, each snapshot  $u_\delta \in \mathcal{S}_g$  can be expanded by the decomposition,

$$(4.6) \quad u_\delta(x, t_\ell; \boldsymbol{\mu}_\ell) = u_\delta(x_*, t_\ell; \boldsymbol{\mu}_\ell) + \sum_{j=1}^J \gamma_{j,\ell} \sigma_j(x, t_\ell; \boldsymbol{\mu}_\ell), \quad \ell = 1, \dots, N_g,$$

for  $x_*$  and  $J$  independent of  $\ell$  and  $\text{sign}(\gamma_{j,\ell}) = \text{sign}(\gamma_{j,\ell'})$  for  $\ell, \ell' = 1, \dots, N_g$ . Then, for a fixed  $j \in \{1, \dots, J\}$ , every pair

$$(4.7) \quad \sigma_j(\cdot, t_\ell; \boldsymbol{\mu}_\ell), \sigma_j(\cdot, t_{\ell'}; \boldsymbol{\mu}_{\ell'}) \in \{\sigma_j(\cdot, t_\ell; \boldsymbol{\mu}_\ell)\}_{\ell=1}^{N_g}$$

yields a specific transport map that is the explicit solution to the Monge-Kantorovich optimal transport problem, called the *monotone rearrangement* [\[34, 35, 22\]](#). We will combine these maps for  $j = 1, \dots, J$  to produce so-called DIP maps.

The DIP maps are constructed as follows. Let us define  $\sigma_j(x) := \sigma_j(x, t_1; \boldsymbol{\mu}_1)$ . Then the rearrangement map from  $(t_1, \boldsymbol{\mu}_1)$  to  $(t_\ell, \boldsymbol{\mu}_\ell)$  is the map  $R_{j,\ell}(x) : \text{supp } \sigma_j' \rightarrow \mathbb{R}$  given by

$$(4.8) \quad R_{j,\ell}(x) := \sigma_j^{-1}(\sigma_j(x), t_\ell; \boldsymbol{\mu}_\ell).$$

Note that  $R_{j,\ell}$  is continuous and piecewise linear: since  $\sigma_j^{-1}(\cdot, t; \boldsymbol{\mu})$  is continuous and piecewise linear,  $R_{j,\ell}$  is a composition of two such maps. So far, the map is only defined in a part of the domain, so we combine these maps for all  $j = 1, \dots, J$ . Let  $\Omega_0 := \cup_{j=1}^J \text{int}(\text{supp } \sigma_j')$ , then let  $R_\ell(x) : \Omega_0 \rightarrow \mathbb{R}$  be defined by

$$(4.9) \quad R_\ell(x) := R_{j(x),\ell}(x)$$

where  $j(x)$  is  $j \in \{1, \dots, J\}$  such that  $x \in \text{int}(\text{supp } \sigma_j')$ . The DIP map is the extension of  $R_\ell$  on the entire real line as defined in the following.

DEFINITION 4.5. *The DIP map  $T_\ell$ ,  $\ell = 1, \dots, N_g$ , is the continuous piecewise linear extension of  $R_\ell$  given in (4.9) to the real line  $\mathbb{R}$  using*

- (1) *continuation at  $\text{int}(\Omega) \setminus \Omega_0$ ,*
- (2) *extrapolation at the boundaries by  $T'_\ell(x) := R'_\ell(x)$  for  $x \in \{x_\ell, x_r\}$ .*

As discussed in [24], it can be shown the DIP map approximates the map generated by the characteristic curves of the scalar conservation law (2.1). A consequence is that DIP between the classical solutions to the homogeneous version of (2.1) at two different times yields the solution at an intermediate time.

**4.3. Low-rank approximation of DIP maps.** The DIP maps  $\{T_\ell\}_{\ell=1}^{N_g}$  can be low-rank, although the collection of functions generated by the composition of the DIP map  $\{T_\ell^\flat \xi : \xi \in \mathbb{V}_{\text{rb}}\}_{\ell=1}^{N_g}$  is high-rank in general (see Figure 4.1). To exploit this low-rank structure, we proceed to compute the low-rank approximation to  $\{T_\ell\}_{\ell=1}^{N_g}$ .

Collecting the DIP maps  $\{T_\ell\}_{\ell=1}^{N_g}$  one can use standard tools, e.g. SVD, to compute a low-rank structure. Let  $\mathbf{T} : \mathbb{R} \rightarrow \mathbb{R}^{N_g}$  with  $(\mathbf{T})_\ell := T_\ell$  then

$$(4.10) \quad v_m(x) = \mathbf{T}(x) \cdot \mathbf{v}_m,$$

where  $\cdot$  is the inner product between two vectors in  $\mathbb{R}^{N_g}$ , and  $\mathbf{v}_m \in \mathbb{R}^{N_g}$ , is the  $m$ -th eigenvector for the matrix  $\mathbf{C} \in \mathbb{R}^{N_g \times N_g}$ , given by the inner products

$$(\mathbf{C})_{\ell, \ell'} := (T_\ell, T_{\ell'}), \quad \ell, \ell' = 1, \dots, N_g.$$

One obtains  $\{v_m\}_{m=1}^M$  if one truncates the eigenfunction expansion after the first  $M$  terms corresponding to the largest eigenvalues.

Note that that  $T_1 = \text{Id}$  and each map  $T_\ell$  contains a component of the identity map, i.e.  $(T_\ell, \text{Id}) \neq 0$ . So it is convenient to let  $v_1 := \text{Id}$  then compute the correlation matrix as of the perturbation from the identity. That is, pre-process  $\mathbf{C}$  to obtain  $\bar{\mathbf{C}} \in \mathbb{R}^{(N_g-1) \times (N_g-1)}$

$$(4.11) \quad (\bar{\mathbf{C}})_{\ell, \ell'} := (T_{\ell+1} - \text{Id}, T_{\ell'+1} - \text{Id}) \quad \text{for } \ell, \ell' = 1, \dots, N_g - 1,$$

then use  $\bar{\mathbf{C}}$  in place of  $\mathbf{C}$  to compute the corresponding basis  $\{v_m\}_{m=2}^M$ . We shall do so in our numerical experiments below.

In what follows, we will denote by  $\{v_m\}_{m=1}^M$  and  $\mathbb{T}_{\text{rb}} \subset \mathbb{T}$  the basis and finite-dimensional subspace constructed in this section.

DEFINITION 4.6. *We will refer to the constructed basis  $\{v_m(x)\}_{m=1}^M$  (4.10) as transport modes. We will denote by  $\mathbb{T}_{\text{rb}}$  the resulting finite-dimensional transport space (Definition 3.3), and we refer to it as the low-rank transport space.*

**4.4. Local basis.** We will briefly discuss how to construct the subspace  $\mathbb{V}_{\text{rb}}$ . Revisiting the diagram in Figure 3.1, we wish to obtain  $\mathbb{V}_{\text{rb}}$  that locally approximates the manifold  $\mathcal{M}_\delta$ . To this end, a collection of snapshots, which we denote by  $\mathcal{S}_1$ , will be drawn from the local manifold. We use the time-parameters  $(t, \boldsymbol{\mu})$  near a small neighborhood of the fixed point  $(t_1, \boldsymbol{\mu}_1) \in \mathcal{H}_g$  (4.4) to obtain the snapshots. Let us denote the finite collection by  $\mathcal{H}_1$ ,

$$(4.12) \quad \mathcal{H}_1 := \{(t_1, \boldsymbol{\mu}_1), \dots, (t_{N_1}, \boldsymbol{\mu}_{N_1})\}.$$

For convenience, we construct  $\mathbb{V}_{\text{rb}}$  by taking as snapshots

$$(4.13) \quad \begin{aligned} u_{\delta, \ell} &:= u_\delta(\cdot, t_\ell; \boldsymbol{\mu}_\ell), & \partial_x f_\ell &:= \partial_x [f(u_\delta(\cdot, t_\ell; \boldsymbol{\mu}_\ell), \cdot; \boldsymbol{\mu}_\ell)], \\ \partial_x u_{\delta, \ell} &:= \partial_x u_\delta(\cdot, t_\ell; \boldsymbol{\mu}_\ell), & \psi_\ell &:= \psi(u_\delta(\cdot, t_\ell; \boldsymbol{\mu}_\ell), \cdot; \boldsymbol{\mu}_\ell), \end{aligned}$$

for each  $(t_\ell, \boldsymbol{\mu}_\ell) \in \mathcal{H}_1$ , instead of only  $u_\delta(\cdot, t_\ell; \boldsymbol{\mu}_\ell)$ . Then let

$$(4.14) \quad \mathcal{S}_1 := \{u_{\delta,\ell}, \partial_x u_{\delta,\ell}, \partial_x f_\ell, \psi_\ell : \ell = 1, \dots, N_1\}.$$

The reduced space  $\mathbb{V}_{\text{rb}}$  is spanned by the first  $N$  left-singular vectors  $\{\zeta_n\}_{n=1}^N$  of the snapshot matrix corresponding to  $\mathcal{S}_1$ .

**5. Online reduced model.** In this section, we introduce methods that allow efficient online computations with the reduced nonlinear approximation (3.9). Compared to the linear case (2.6), additional considerations are necessary due to the nonlinear aspects of the approximation (3.9).

First, we introduce moving interpolation points we call *interpolation particles*. The motivation is to take advantage of the approximation (3.9), by making these particles move depending on  $(t, \boldsymbol{\mu}) \in \mathcal{H}$  via the transport maps  $\hat{T}_{(t,\boldsymbol{\mu})} \in \mathbb{T}_{\text{rb}}$  constructed in subsection 4.3. We will show that they enable a straightforward change of basis, yielding an efficient projection into the transported subspaces  $\mathbb{V}_{\text{rb}}(t, \boldsymbol{\mu})$  (Definition 3.10). The idea is applied in particular to the empirical interpolation method (EIM/DEIM [2, 5]).

Then we introduce an online time-stepping reduced model for the problem (2.1). It alternates between the update of the local basis coefficients  $\{\beta_n(t, \boldsymbol{\mu})\}_{n=1}^N$  and the update of the nonlinear transport mode coefficients  $\{\alpha_m(t, \boldsymbol{\mu})\}_{m=1}^M$ . The cost of time-stepping the nonlinear reduced model only depends on the reduced degree of freedoms  $N$  and  $M$ , and does not depend on the size of the full model  $N_\delta$  at each time-step.

**5.1. Interpolation particles.** To deal with nonlinear functions in our problem (2.1) as well as function compositions in (3.9) in an efficient manner, we introduce a moving interpolation method that is compatible with empirical interpolation. In the traditional empirical interpolation, one uses the basis functions  $\{\zeta_n\}_{n=1}^N$  of  $\mathbb{V}_{\text{rb}}$  and the corresponding interpolation points  $\mathcal{X} := \{x_i\}_{i=1}^N \subset \Omega$ . We generalize the pair  $\{\zeta_n\}_{n=1}^N$  and  $\{x_i\}_{i=1}^N$  by allowing the interpolation to move according to the transport map  $\hat{T}_{(t,\boldsymbol{\mu})} \in \mathbb{T}_{\text{rb}}$ . As a result, one obtains a collection of pairs: the transported basis  $\{\hat{T}_{(t,\boldsymbol{\mu})}^\flat \zeta_n\}_{n=1}^N$  and the corresponding interpolation points  $\hat{T}_{(t,\boldsymbol{\mu})}(\mathcal{X})$ .

Hence, the transport evolves the interpolation points over time, effectively endowing these points with momenta. So we will refer to these interpolation points  $\hat{T}_{(t,\boldsymbol{\mu})}(\mathcal{X})$  that move along the transport as *interpolation particles*.

**DEFINITION 5.1.** *Given a basis  $\{\zeta_n\}_{n=1}^N$  that spans  $\mathbb{V}_{\text{rb}}$  and its interpolation points  $\mathcal{X} = \{x_i\}_{i=1}^N \subset \Omega$ , the interpolation particles for the basis  $\{\hat{T}_{(t,\boldsymbol{\mu})}^\flat \zeta_n\}_{n=1}^N$  of  $\mathbb{V}_{\text{rb}}(t, \boldsymbol{\mu})$  is defined as  $\hat{T}_{(t,\boldsymbol{\mu})}(\mathcal{X})$ .*

Onwards, we will refer to the interpolation particles simply as particles. A useful property is that the empirical interpolation construction commutes with the transport operation.

**PROPOSITION 5.2.** *Given a basis  $\{\zeta_n\}_{n=1}^N$  and corresponding interpolation points  $\mathcal{X} = \{x_i\}_{i=1}^N \subset \Omega$ , assume  $\hat{T}_{(t,\boldsymbol{\mu})} \in \mathbb{T}_{\text{rb}} \sqsubset \mathbb{T}$  and that  $\hat{T}_{(t,\boldsymbol{\mu})}(\mathcal{X}) \subset \Omega$ . Then the particles  $\hat{T}_{(t,\boldsymbol{\mu})}(\mathcal{X})$  are the interpolation points of  $\{\hat{T}_{(t,\boldsymbol{\mu})}^\flat \zeta_n\}_{n=1}^N$ .*

*Proof.* For simplicity denote  $\hat{T} := \hat{T}_{(t,\boldsymbol{\mu})}$  for a fixed  $(t, \boldsymbol{\mu}) \in \mathcal{H}$  during this proof. For  $x_i \in \mathcal{X}$ ,

$$(5.1) \quad \hat{T}^\flat \zeta_n(\hat{T}(x_i)) = \zeta_n(\hat{T}^{-1}(\hat{T}(x_i))) = \zeta_n(x_i) \quad \text{for } i = 1, 2, \dots, N,$$

which implies that

$$(5.2) \quad \operatorname{argmax}_{x \in \Omega} |\hat{T}^b \zeta_n(x)| = \hat{T}(\operatorname{argmax}_{x \in \hat{T}(\Omega)} |\zeta_n(x)|).$$

Then we show by induction that the interpolation points of the basis  $\{\hat{T}^b \zeta_n\}_{n=1}^N$  is equal to  $\hat{T}^b(\mathcal{X})$ . Let us denote by  $\{\tau_1, \dots, \tau_I\}$  the interpolation points corresponding to  $\{\hat{T}^b \zeta_1, \dots, \hat{T}^b \zeta_I\}$  for  $I \leq N$ . When  $I = 1$ ,

$$(5.3) \quad \tau_1 = \operatorname{argmax}_{x \in \Omega} |\hat{T}^b \zeta_1(x)| = \hat{T}(\operatorname{argmax}_{x \in \hat{T}(\Omega)} |\zeta_1(x)|) = \hat{T}(x_1).$$

Suppose  $\tau_i = \hat{T}(x_i)$  for  $i = 1, 2, \dots, I - 1$ . Then upon solving for  $\{\vartheta_n\}_{n=1}^{I-1}$  in

$$(5.4) \quad \sum_{n=1}^{I-1} \vartheta_n^{I-1} \hat{T}^b \zeta_n(\tau_i) = \hat{T}^b \zeta_I(\tau_i) \quad \text{for } i = 1, 2, \dots, I - 1,$$

the next interpolation point  $\tau_I$  is found by

$$(5.5) \quad \tau_I = \operatorname{argmax}_{x \in \Omega} |\hat{T}^b \zeta_I(x) - \sum_{n=1}^{I-1} \vartheta_n^{I-1} \hat{T}^b \zeta_n(x)|.$$

Observe that (5.4) and (5.5) can be re-written in terms of the next interpolation point  $x_I$  of  $\{\zeta_n\}_{n=1}^I$ . That is, since  $\{\vartheta_n\}_{n=1}^{I-1}$  also satisfy,

$$(5.6) \quad \sum_{n=1}^{I-1} \vartheta_n^{I-1} \zeta_n(x_i) = \zeta_I(x_i) \quad \text{for } i = 1, 2, \dots, I - 1,$$

one may re-write (5.5) and obtain

$$(5.7) \quad \tau_I = \hat{T}(\operatorname{argmax}_{x \in \hat{T}(\Omega)} |\zeta_I(x) - \sum_{n=1}^{I-1} \vartheta_n^{I-1} \zeta_n(x)|) = \hat{T}(x_I).$$

Therefore  $\tau_i = \hat{T}(x_i)$  for all  $i = 1, 2, \dots, N$ .  $\square$

Moreover, it is efficient to compute the derivatives of  $\xi \in \mathbb{V}_{\text{rb}}(t, \boldsymbol{\mu})$  at the particles locations  $\hat{T}_{(t, \boldsymbol{\mu})}(\mathcal{X})$ .

**PROPOSITION 5.3.** *If  $\xi \in \mathbb{V}_{\text{rb}}(t, \boldsymbol{\mu})$  then  $\frac{d\xi}{dx}(\hat{T}_{(t, \boldsymbol{\mu})}(x_i))$  for each  $x_i \in \mathcal{X}$  can be computed in  $\mathcal{O}(N + M)$  operations.*

*Proof.* Since  $\xi \in \mathbb{V}_{\text{rb}}(t, \boldsymbol{\mu})$ , we have  $\frac{d\xi}{dx}(x) = \sum_{n=1}^N \vartheta_n (\frac{d}{dx} \hat{T}_{(t, \boldsymbol{\mu})}^b \zeta_n(x))$ . Furthermore, the derivative  $\frac{d}{dx} \hat{T}_{(t, \boldsymbol{\mu})}^b \zeta_n$  at the particle location  $\hat{T}_{(t, \boldsymbol{\mu})}(x_i)$  is given by the chain rule,

$$(5.8) \quad \frac{d}{dx} \hat{T}_{(t, \boldsymbol{\mu})}^b \zeta_n(\hat{T}_{(t, \boldsymbol{\mu})}(x_i)) = \frac{1}{\hat{T}'_{(t, \boldsymbol{\mu})}(x_i)} \frac{d\zeta_n}{dx}(x_i) \quad \text{for } i, n = 1, \dots, N.$$

Since  $\hat{T}_{(t, \boldsymbol{\mu})} \in \operatorname{span}\{v_m\}_{m=1}^M$  (3.9), its derivative at the particle locations is

$$(5.9) \quad \frac{d}{dx} \hat{T}_{(t, \boldsymbol{\mu})}(x_i) = \sum_{m=1}^M \alpha_m(t, \boldsymbol{\mu}) v'_m(x_i) \quad \text{for } i = 1, \dots, N.$$

Thus  $\frac{d\xi}{dx}(x_i)$  is computed in  $2(N + M) - 1$  operations, that is,  $\mathcal{O}(N + M)$ .  $\square$

*Remark 5.4.* In computing  $\frac{d\xi}{dx}(\hat{T}_{(t, \boldsymbol{\mu})}(x_i))$  the values  $\{\frac{d\zeta_n}{dx}(x_i)\}_{n=1}^N, \{v'_m(x_i)\}_{m=1}^M$  do not depend on  $(t, \boldsymbol{\mu}) \in \mathcal{H}$ . They can be pre-computed during the offline stage.

**5.2. Change of basis.** When the transport map  $\hat{T}_{(t,\mu)}$  and therefore  $\mathbb{V}_{\text{rb}}(t, \mu)$  is updated, the approximation (3.9) allows a simple change of basis procedure with computational effort of  $\mathcal{O}(N + M)$  and does not require expensive calculations that depend on the size of the full model  $N_\delta$ .

Here we describe how to perform the change of basis: Given the local basis  $\mathbb{V}_{\text{rb}} \subset \mathbb{V}_\delta$ , interpolation points  $\mathcal{X} = \{x_i\}_{i=1}^N$ , transport maps  $\hat{T}_{(1)}, \hat{T}_{(2)} \in \mathbb{T}_{\text{rb}}$  and corresponding particles  $\hat{T}_{(1)}(\mathcal{X}) = \{x_i^{(1)}\}_{i=1}^N$ ,  $\hat{T}_{(2)}(\mathcal{X}) = \{x_i^{(2)}\}_{i=1}^N$ , suppose  $u^{(1)} \in \mathbb{V}_{\text{rb}}(\hat{T}_{(1)})$  and we wish compute  $u^{(2)} \in \mathbb{V}_{\text{rb}}(\hat{T}_{(2)})$ , satisfying  $u^{(1)}(x_i^{(2)}) = u^{(2)}(x_i^{(2)})$  for all  $i = 1, \dots, N$ .

Writing  $u^{(1)}, u^{(2)}$  and  $T^{(1)}, T^{(2)}$  as

$$(5.10) \quad \begin{aligned} u^{(1)}(x) &= \sum_{n=1}^N \beta_n^{(1)} \hat{T}_{(1)}^b \zeta_n(x), & \hat{T}_{(1)}(x) &= \sum_{m=1}^M \alpha_m^{(1)} v_m(x), \\ u^{(2)}(x) &= \sum_{n=1}^N \beta_n^{(2)} \hat{T}_{(2)}^b \zeta_n(x), & \hat{T}_{(2)}(x) &= \sum_{m=1}^M \alpha_m^{(2)} v_m(x), \end{aligned}$$

it is clear that, to determine  $u^{(2)}(x)$  it suffices to compute its coefficients  $\{\beta_n^{(2)}\}_{n=1}^N$ . Moreover, if we can compute the values  $u^{(1)}(x_i^{(2)})$  then by empirical interpolation we can solve for  $\{\beta_n^{(2)}\}_{n=1}^N$  in

$$(5.11) \quad \sum_{n=1}^N \beta_n^{(2)} \hat{T}_{(1)}^b \zeta_n(x_i^{(2)}) = \sum_{n=1}^N \beta_n^{(2)} \zeta_n(x_i) = u^{(1)}(x_i^{(2)}), \quad \text{for } i = 1, \dots, N,$$

and therefore the desired approximation  $u^{(2)}(x)$ . So it remains to evaluate  $u^{(1)}$  at  $x_i^{(2)}$ , or equivalently,  $\hat{T}_{(1)}^b \zeta_n$  at  $x_i^{(2)}$ .

Note that  $u^{(1)} \notin \mathbb{V}_\delta$ , i.e. it is piecewise linear on a non-uniform grid, thus evaluating it at an arbitrary point  $x_i^{(2)} \in \Omega$  is a non-trivial operation. But if  $x_i^{(1)}, x_i^{(2)}$  are close enough, the evaluation only involves local calculations on the uniform grid.

**PROPOSITION 5.5.** *If  $0 < \pm(\hat{T}_{(1)}^{-1}(x_i^{(2)}) - x_i) < \delta$  then*

$$(5.12) \quad \hat{T}_{(1)}^b \zeta_n(x_i^{(2)}) = \zeta_n(x_i) + \zeta_n'(x_i^\pm) (\hat{T}_{(1)}^{-1}(x_i^{(2)}) - x_i),$$

in which  $x_i^-, x_i^+$  refers to left and right limits.

*Proof.* This follows directly from the fact that  $\zeta_n \in \mathbb{V}_\delta$  so it is continuous and piecewise linear on a uniform grid.  $\square$

The values  $\zeta_n(x_i), \zeta_n'(x_i^\pm)$  are already known and do not depend on the transport maps. Hence  $u^{(1)}(x_i^{(2)})$  can be computed using pre-computed values near the particles.

Note that if  $x_i^{(2)}$  lies further away from  $x_i^{(1)}$ , one can compute additional corrections to (5.12) to obtain the exact value of  $\hat{T}_{(1)}^b \zeta_n(x_i^{(2)})$ . Moreover, in case a basis  $\{\zeta_n\}_{n=1}^N$  of higher-order polynomial degree was given, straightforward corrections can be made to (5.12).

**5.3. Online reduced-model time-update.** In this section, we discuss an online efficient evaluation of the reduced model by time-stepping. We build on the first order Godunov flux updates and employ Godunov splitting for the source term here, but other schemes are possible following similar steps as below.

During the evaluation,  $\boldsymbol{\mu}$  is fixed in our PDE (2.1), so we will omit the dependence on the parameter on  $\boldsymbol{\mu}$  by writing, e.g.  $\hat{u}(x, t) = \hat{u}(x, t; \boldsymbol{\mu})$ ,  $f(u, x) = f(u, x; \boldsymbol{\mu})$ ,  $\psi(u, x) = \psi(u, x; \boldsymbol{\mu})$ ,  $\hat{T}_t = \hat{T}_{(t, \boldsymbol{\mu})}$ ,  $\mathbb{V}_{\text{rb}}(t) = \mathbb{V}_{\text{rb}}(t, \boldsymbol{\mu})$ ,  $\alpha(t) = \alpha(t, \boldsymbol{\mu})$ ,  $\beta(t) = \beta(t, \boldsymbol{\mu})$ ,  $\mathcal{X}(t) = \mathcal{X}(t, \boldsymbol{\mu})$ .

We then write our reduced-model approximation in a time-discrete form, by discretizing the time variable by uniform time-steps  $0 =: t_0 < t_1 < \dots < t_K := t_F$ . Extension to adaptive time-steps would be straightforward. Upon writing  $\hat{T}_{(k)} = \hat{T}_{t_k}$ ,  $\mathbb{V}_{\text{rb}}^{(k)} = \mathbb{V}_{\text{rb}}(t_k)$ ,  $\alpha_n^{(k)} = \alpha_n(t_k)$ ,  $\beta_n^{(k)} = \beta_n(t_k)$ ,  $\mathcal{X}^{(k)} = \mathcal{X}(t_k)$ , our fully discrete reduced-model approximation becomes

$$(5.13) \quad \hat{u}_{(k)}(x) = \sum_{n=1}^N \beta_n^{(k)} \hat{T}_{(k)}^b \zeta_n(x), \quad \hat{T}_{(k)}(x) = \sum_{m=1}^M \alpha_m^{(k)} v_m(x),$$

and corresponding particles are denoted by  $\mathcal{X}^{(k)} = \{x_i^{(k)}\}_{i=1}^N$ . The continuous approximation  $\hat{u}(x, t)$  (3.9) can be constructed as the continuous piecewise linear interpolant satisfying  $\hat{u}(x, t_k) = \hat{u}_{(k)}(x)$ .

The reduced-model time-update during the online stage comprises 3 steps:

- (S1) **Evolution of the PDE.** Update the solution  $\{\beta_n^{(k)}\}_{n=1}^N$  to  $\{\bar{\beta}_n^{(k+1)}\}_{n=1}^N$  using the PDE while keeping the transport subspace  $\mathbb{V}_{\text{rb}}^{(k)}$  fixed.
- (S2) **Update of the transport map.** Update  $\hat{T}_{(k)}$  to  $\hat{T}_{(k+1)}$ , that is,  $\{\alpha_m^{(k)}\}_{m=1}^M$  to  $\{\alpha_m^{(k+1)}\}_{m=1}^M$ . This forms the new transported subspace  $\mathbb{V}_{\text{rb}}^{(k+1)}$ .
- (S3) **Change of basis.** Compute  $\{\beta_n^{(k+1)}\}_{n=1}^N$  from  $\{\alpha_m^{(k+1)}\}_{m=1}^M$  and  $\{\bar{\beta}_n^{(k+1)}\}_{n=1}^N$  by a change of basis where the evolved solution is projected onto the new transported subspace  $\mathbb{V}_{\text{rb}}^{(k+1)}$ .

We detail each step in individual subsections below. A concise algorithmic description of the time-update is given in [section 6](#).

**5.3.1. Evolution of the PDE.** In the first step (S1), we update the coefficients  $\beta_n^{(k)}$  to  $\bar{\beta}_n^{(k+1)}$  while keeping the transport map  $\hat{T}_{(k)}$  fixed. This is done by evolving the PDE forward using a Godunov splitting (see [12]): First we perform the flux update using the Godunov flux, then the source update by adding the contribution from the nonlinear source term. In both cases, the update is projected to the transported basis  $\mathbb{V}_{\text{rb}}^{(k)}$ . The evolution steps follows in 2 stages (S1.1) and (S1.2).

During the flux update the intermediate step  $u_*(x)$  with coefficients  $\{\beta_n^*\}_{n=1}^N$  is obtained by adding the flux contribution,

$$(S1.1) \quad \beta_n^* = \beta_n^{(k)} + \lambda \theta_n^{(k)}, \quad \text{for } n = 1, \dots, N,$$

where  $\theta_n^{(k)}$  arises from the flux term  $\partial_x f$  in the PDE (2.1).

Then the source update is given by

$$(S1.2) \quad \bar{\beta}_n^{(k+1)} = \beta_n^* + \Delta t \gamma_n^{(k)} \quad \text{for } n = 1, \dots, N,$$

where  $\gamma_n^{(k)}$  corresponds to the source term  $\psi$  in the PDE (2.1).

In the remainder of this section, we will discuss how to compute the contributions  $\{\theta_n^{(k)}\}_{n=1}^N$  and  $\{\gamma_n^{(k)}\}_{n=1}^N$  using empirical interpolation.

The desired flux update is given by

$$(5.14) \quad u_*(x) = \hat{u}_{(k)}(x) - \lambda \Delta \mathcal{F}(\hat{u}_{(k)}(x), x),$$

where  $\lambda = \Delta t / \Delta x$  is the ratio between the size of the time-step and the spatial grid-width of the full model (with uniform spacing  $\Delta x = \delta$ ), and the numerical flux difference  $\Delta \mathcal{F}$  is given by the upwind flux,

$$(5.15) \quad \Delta \mathcal{F}(\hat{u}_{(k)}(x), x) := f(\hat{u}_{(k)}(x), x) - f(\hat{u}_{(k)}(x - \Delta x), x - \Delta x).$$

To approximate the flux difference  $-\Delta \mathcal{F}(\hat{u}_{(k)}(x), x)$  using the basis  $\{\hat{T}_{(k)}^b \zeta_n\}_{n=1}^N$  by empirical interpolation, we impose that the two agree at the particles  $\{x_i^{(k)}\}_{i=1}^N$ ,

$$(5.16) \quad \sum_{n=1}^N \theta_n^{(k)} \hat{T}_{(k)}^b \zeta_n(x_i^{(k)}) = -\Delta \mathcal{F}(\hat{u}_{(k)}(x_i^{(k)}), x_i^{(k)}) \quad \text{for } i = 1, \dots, N.$$

That is, one solves for the coefficients  $\{\theta_n^{(k)}\}_{n=1}^N$  in the system

$$(5.17) \quad \sum_{n=1}^N \theta_n^{(k)} \zeta_n(x_i) = -\Delta \mathcal{F}(\hat{u}_{(k)}(x_i^{(k)}), x_i^{(k)}) \quad \text{for } i = 1, \dots, N.$$

The flux difference  $\Delta \mathcal{F}(\hat{u}_{(k)}(x_i^{(k)}), x_i^{(k)})$  is then approximated by  $f_{\ell,i}^{(k)} - f_{r,i}^{(k)}$  in which

$$(5.18) \quad \begin{aligned} f_{\ell,i}^{(k)} &:= f\left(\sum_{n=1}^N \beta_n^{(k)} (\zeta_n(x_i) - \frac{d}{dx} \hat{T}_{(k)}^b \zeta_n(x_i^{(k)}) \Delta x), x_i^{(k)} - \Delta x\right), \\ f_{r,i}^{(k)} &:= f\left(\sum_{n=1}^N \beta_n^{(k)} \zeta_n(x_i), x_i^{(k)}\right). \end{aligned}$$

The derivative in the first term can be computed using [Proposition 5.3](#). This concludes the computation of  $\{\theta_n^{(k)}\}_{n=1}^N$ .

Next, we compute the contribution from the source term  $\psi(u_*(x), x)$ . To approximate the contribution in  $\text{span}\{\hat{T}_{(k)}^b \zeta_n\}_{n=1}^N$  using empirical interpolation, we solve the system

$$(5.19) \quad \sum_{n=1}^N \gamma_n^{(k)} \zeta_n(x_i) = \psi(u_*(x_i^{(k)}), x_i^{(k)}) \quad \text{for } i = 1, \dots, N.$$

This yields the coefficients  $\{\gamma_n^{(k)}\}_{n=1}^N$ .

Having updated  $\{\beta_n^{(k)}\}_{n=1}^N$  to  $\{\bar{\beta}_n^{(k+1)}\}_{n=1}^N$  we let

$$(5.20) \quad \bar{u}_{(k+1)}(x) := \sum_{n=1}^N \bar{\beta}_n^{(k+1)} \hat{T}_{(k)}^b \zeta_n(x).$$

This completes the first step.

**5.3.2. Update of the transport map.** In the second step (S2), we determine the appropriate subsequent transport map  $\hat{T}_{(k+1)}$ , that is, we update the transport mode coefficients  $\{\alpha_m^{(k)}\}_{m=1}^M$  to  $\{\alpha_m^{(k+1)}\}_{m=1}^M$ . The update is given by

$$(S2) \quad \alpha_m^{(k+1)} = \alpha_m^{(k)} + \Delta t \eta_m^{(k)} \quad \text{for } m = 1, \dots, M.$$

The contribution  $\{\eta_m^{(k)}\}_{m=1}^M$  is obtained by solving a system of equations for a subset  $\mathcal{Q} = \{x_{i_j}\}_{j=1}^M \subset \mathcal{X}$ ,

$$(5.21) \quad \sum_{m=1}^M \eta_m^{(k+1)} v_m(x_{i_j}) = - \left( \frac{\bar{u}_{(k+1)}(x_{i_j}^{(k)}) - \hat{u}_{(k)}(x_{i_j}^{(k)})}{\partial_x \hat{u}_{(k)}(x_{i_j}^{(k)})} \right) \quad \text{for } j = 1, \dots, M.$$

We will now derive the update (S2) and discuss the choice of  $\mathcal{Q} \subset \mathcal{X}$ . For each interpolation particle  $x_i^{(k)} \in \mathcal{X}^{(k)}$ , we employ the following update,

$$(5.22) \quad x_i^{(k+1)} = x_i^{(k)} - \Delta t \chi_i^{(k)}, \quad \chi_i^{(k)} := \left( \frac{\partial_t \hat{u}(x_i^{(k)}, t_k)}{\partial_x \hat{u}(x_i^{(k)}, t_k)} \right), \quad i = 1, \dots, N.$$

The term  $\chi_i^{(k)}$  can be approximated by our time-update  $\bar{u}_{(k+1)}(x)$  detailed in the previous step,

$$(5.23) \quad \frac{\bar{u}_{(k+1)}(x_i^{(k)}) - \hat{u}_{(k)}(x_i^{(k)})}{\partial_x \hat{u}_{(k)}(x_i^{(k)})}.$$

Computing the transport mode coefficients of this term via empirical interpolation using  $\mathcal{Q}$  as interpolation points results in the formula (5.21).

Next, we discuss how to choose  $M$  points  $\mathcal{Q} \subset \mathcal{X}$ . We will assume  $N > M$  and select a subset of  $\mathcal{X}$  to serve as interpolation points for  $\{v_m\}_{m=1}^M$ . This assumption is not restrictive, since in the case  $N \leq M$  similar procedures can be devised. We choose the subset that greedily maximizes the amplitude of  $\partial_x \hat{u}_{(0)}$ . Let  $Q_j := \{x_{i_1}, \dots, x_{i_j}\}$  and let  $Q_0 := \emptyset$ , then for  $j = 1, \dots, M$ ,

$$(5.24) \quad i_j := \operatorname{argmax}_i \{ |\partial_x \hat{u}|(x_i, t_0) : x_i \in \mathcal{X} \setminus Q_{j-1} \}.$$

The subset  $\mathcal{Q} := Q_M = \{x_{i_j}\}_{j=1}^M$  are to be used with  $\{v_m\}_{m=1}^M$ .

*Remark 5.6.* The choice of  $\mathcal{Q}$  is critical and although we provided a heuristic procedure we use in our numerical examples, it is an open problem as to which points in the domain  $\mathcal{Q} \subset \Omega$  are optimal to choose. Note that the update (5.22) is motivated by the characteristic curves to the problem (2.1).

**5.3.3. Change of basis.** In the third and final step (S3), we close the time-update loop via a change of basis discussed in the subsection 5.2, by computing  $\hat{u}_{(k+1)}(x)$  from  $\bar{u}_{(k+1)}(x)$ , that is,  $\{\beta_n^{(k+1)}\}_{n=1}^N$  from  $\{\bar{\beta}_n^{(k+1)}\}_{n=1}^N$  in

$$(S3) \quad \begin{aligned} \hat{u}_{(k+1)}(x_i^{(k+1)}) &= \sum_{n=1}^N \beta_n^{(k+1)} \hat{T}_{(k+1)}^b \zeta_n(x_i^{(k+1)}) \\ &= \sum_{n=1}^N \beta_n^{(k+1)} \zeta_n(x_i) = \sum_{n=1}^N \bar{\beta}_n^{(k+1)} \hat{T}_{(k)}^b \zeta_n(x_i^{(k+1)}), \quad i = 1, \dots, N. \end{aligned}$$

We remark that the finite propagation speed of (2.1) and the CFL restriction for the full model implies that the interpolation particles  $\{x_i^{(k+1)}\}_{i=1}^N$  should not move more than one full-model grid-width  $\delta$  at each time-step, although this is not rigorously guaranteed for the online reduced model.



**5.4. Reconstruction of the reduced solution.** As a result of the online computations, we obtain two sets of coefficients in (3.9), namely  $\{\alpha_m^{(k)}\}_{m=1}^M$  and  $\{\beta_n^{(k)}\}_{n=1}^N$  for  $k = 0, 1, \dots, K$ . To utilize this reduced-model solution, one can reconstruct the solution on the full-model grid, and evaluate it to desired accuracy. While this reconstruction procedure does depend on the full-model degree of freedom  $N_\delta$ , it can be computed in an embarrassingly parallel manner in both space and time: for each spatial point on the full-model grid and for each time.

**6. Algorithms.** In this section, we provide a concise summary of the MATS algorithm introduced above. The offline computations are given in Algorithm 6.1 and the online computations in Algorithm 6.2.

---

**Algorithm 6.1** MATS Offline

---

Compute basis  $\{v_m\}_{m=1}^M$  of  $\mathbb{T}_{\text{rb}}$

1. Collect snapshots  $\mathcal{S}_g$  satisfying the signature condition from full model
2. Compute DIP maps  $\{T_\ell\}_{\ell=1}^{N_g}$
3. Compute low-rank transport modes  $\{v_m\}_{m=1}^M$  from  $\{T_\ell\}_{\ell=1}^{N_g}$  via SVD

Compute basis  $\{\zeta_n\}_{n=1}^N$  of  $\mathbb{V}_{\text{rb}}$

1. Collect snapshots  $\mathcal{S}_l$  from local time-parameter region from full model
  2. Compute reduced basis  $\{\zeta_n\}_{n=1}^N$  from  $\mathcal{S}_l$  via SVD
  3. Compute interpolation points  $\{x_i\}_{i=1}^N$  via EIM/DEIM
- 

**7. Numerical examples.** We will demonstrate the methods discussed in the previous sections through two representative examples. One is the color equation with parametrized variable speed, and the other is the Burgers' equation with a parametrized source term. Throughout, we will denote by  $N$  and  $M$  the dimensions of our reduced model (3.9),  $N = \dim \mathbb{V}_{\text{rb}}$ ,  $M = \dim \mathbb{T}_{\text{rb}}$ .

**7.1. Color equation with parameter-dependent heterogeneous media.**

Let us consider the color equation with parametrized variable speed that is smooth,

$$(7.1) \quad \begin{cases} \partial_t u + c(x; \boldsymbol{\mu}) \partial_x u = 0 & (x, t) \in (0, 2) \times (0, 1) \\ u(x, 0) = u_0(x), \\ u(0, t) = u_0(0). \end{cases}$$

The initial condition is the cosine hump of width 0.4 centered at  $x = 0.25$ ,

$$(7.2) \quad u_0(x) := \begin{cases} 0 & \text{if } x < 0.05 \text{ or } x > 0.45, \\ \frac{1}{2} + \frac{1}{2} \cos(5\pi(x - 0.25)) & \text{if } 0.05 \leq x \leq 0.45. \end{cases}$$

This is a problem of the type (2.1) with  $f(u, x; \boldsymbol{\mu}) = c(x; \boldsymbol{\mu})u$ ,  $\psi(u, x; \boldsymbol{\mu}) = c_x(x; \boldsymbol{\mu})u$ .

The variable speed  $c(\cdot; \boldsymbol{\mu})$  defined as a modulation of a constant background speed by a mixture of two parameter-dependent harmonic functions,

$$c(x; \boldsymbol{\mu}) = 1.5 + \mu_1 \sin(\mu_2 x) + 0.1 \cos(\mu_3 x).$$

The parameters  $\mu_2$  and  $\mu_3$  correspond to fast and slow oscillations, respectively, and  $\mu_1$  controls the amplitude of the fast oscillation. We choose the parameter domain  $\mathcal{D} := [0.25, 0.5] \times [2\pi, 6\pi] \times [\pi, 1.1\pi]$ . One can numerically check that for this problem the signature condition (Definition 4.4) is satisfied by the full model (see Remark 4.1).

---

**Algorithm 6.2** MATS Online
 

---

 Initialize  $\{\alpha_m^{(0)}\}_{m=1}^M, \{\beta_n^{(0)}\}_{n=1}^N, \{x_i^{(0)}\}_{i=1}^N, \hat{T}_{(0)} \leftarrow \sum_{m=1}^M \alpha_m^{(0)} v_m, \lambda \leftarrow \Delta t / \Delta x$ 

 Time-step for  $k = 0, \dots, K$ 

1. Compute flux
- $\{\theta_n^{(k)}\}_{n=1}^N$
- , then compute flux update

$$(S1.1) \quad \beta_n^* \leftarrow \beta_n^{(k)} + \lambda \theta_n^{(k)}, \quad n = 1, \dots, N.$$

 Compute source  $\{\gamma_n^{(k)}\}_{n=1}^N$ , then compute source update

$$(S1.2) \quad \bar{\beta}_n^{(k+1)} \leftarrow \beta_n^* + \Delta t \gamma_n^{(k)}, \quad n = 1, \dots, N.$$

2. Compute
- $\{\eta_m^{(k)}\}_{m=1}^M$
- , then compute transport map update

$$(S2) \quad \alpha_m^{(k+1)} \leftarrow \alpha_m^{(k)} + \Delta t \eta_m^{(k)}, \quad m = 1, \dots, M,$$

$$\hat{T}_{(k+1)} \leftarrow \sum_{m=1}^M \alpha_m^{(k+1)} v_m,$$

$$x_i^{(k+1)} \leftarrow \hat{T}_{(k+1)}(x_i), \quad i = 1, \dots, N.$$

3. Change of basis

$$(S3) \quad \beta_n^{(k+1)} \leftarrow \text{SOLVE} \left[ \begin{array}{l} \sum_{n=1}^N \beta_n^{(k+1)} \zeta_n(x_i) = \sum_{n=1}^N \bar{\beta}_n^{(k+1)} \hat{T}_{(k)}^b \zeta_n(x_i^{(k+1)}) \\ i = 1, \dots, N. \end{array} \right]$$


---

Our strategy for collecting snapshots is to (1) choose random samples for the parameter  $\boldsymbol{\mu} \in \mathcal{D}$ , and (2) pick two time-intervals, one local (near initial time) and one global. Then the full-model solutions computed for randomly drawn  $\boldsymbol{\mu}$ : Solutions for the local time-interval will form the local snapshots and those for global time-intervals, the global snapshots.

We pick random parameters  $\boldsymbol{\mu}$  by drawing 25 independent and uniformly distributed random samples in the domain  $\mathcal{D}$ . We denote the set of these samples to be  $\mathcal{N}_1$ , see [Figure 7.2](#) for a scatter plot. Local snapshots computed with the full model are taken from equally spaced times in  $[0, 0.05]$  near the initial time. Then the local snapshots are taken for time-parameter values

$$\mathcal{H}_1 := \{(t, \boldsymbol{\mu}) : t \in \mathcal{T}_1, \boldsymbol{\mu} \in \mathcal{N}_1\}, \quad \mathcal{T}_1 := \{0.02i : i = 0, 1, \dots, 4\}.$$

Hence, we obtain the local snapshots  $\mathcal{S}_l$  (4.14) of size  $|\mathcal{S}_l| = 125$ .

Similarly, global snapshots  $\mathcal{S}_g$  are taken over longer periods of time,

$$\mathcal{H}_g := \mathcal{H}_1 \cup \{(t, \boldsymbol{\mu}) : t \in \mathcal{T}_g, \boldsymbol{\mu} \in \mathcal{N}_1\}, \quad \mathcal{T}_g := \{0.1i : i = 1, 2, \dots, 10\},$$

yielding the global snapshots  $\mathcal{S}_g$  (4.5) of size  $|\mathcal{S}_g| = 375$ .

For the reduced model, we choose a uniform time-step size with a fixed ratio  $\lambda = \Delta t / \Delta x = 0.5$ . The reduced model is run up to  $K = 2400$  time-steps.

Speedup results shown in [Figure 7.1](#) reflect the theoretical complexity of  $\mathcal{O}(N)$  per time-step, where the runtime is independent of the size of the full model. This

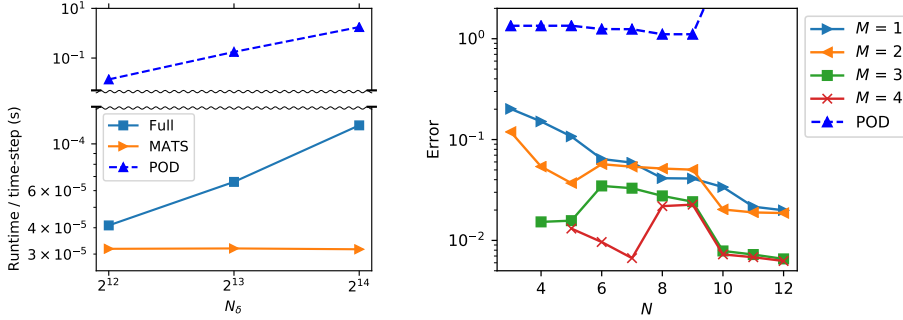


FIG. 7.1. Runtime comparison for single time-step of full model of varying size  $N_\delta$  and corresponding reduced model of dimensions  $(N, M) = (12, 4)$ , POD-DEIM for similar accuracy (left). Average relative error plot for the color equation example (7.1) with various dimensions  $(N, M)$  (right). All implementations are in PYTHON.

is in contrast to the  $\mathcal{O}(N_\delta)$  of the full-model solution, as well as the reduced model employing POD-DEIM that achieves comparable accuracy.

We draw 10 test parameters from a uniform random distribution on  $\mathcal{D}$  (see Figure 7.2) and compare the reconstruction with the full model. The average  $L^1$  relative error between the reduced model and the full model was computed every 100 time-steps for each test parameter. The result for individual test parameter for dimensions  $(N, M) = (12, 4)$  is shown in Figure 7.2: The error over small initial time period is below  $10^{-3}$ , but the error accumulates over time and can reach  $10^{-2}$ . Next, we vary the dimensions  $(N, M)$  and compute the average error over the 10 test parameter samples. The result is shown in Figure 7.1 and serves as numerical evidence that the  $(N, M)$ -width for the problem (7.1) is small. The general trend is that for higher  $(N, M)$  the error decreases, however this trend is not strictly monotone, especially with respect to  $N$ .

A plot of the reduced and full-model solutions, together with the speed  $c(x; \boldsymbol{\mu})$  and the trajectory of the particles are shown in Figure 7.3, demonstrating good agreement between the reduced model and the full model.

**7.2. Burgers' equation with reaction source.** Let us consider a nonlinear example, a Burgers' equation coupled with a reactive equation. This is a model equation for the combustion problem where chemical reaction occurs inside fluid flow (see, e.g. [11]),

$$(7.3) \quad \begin{cases} \partial_t u + \partial_x \left( \frac{1}{2} u^2 \right) = \mu_1 u(1-u)(u-\mu_2), & (x, t) \in (-5, 5) \times (0, t_S(\boldsymbol{\mu})) \\ u(x, 0) = u_0(x), \\ u(0, t) = u_0(0). \end{cases}$$

The first parameter  $\mu_1$  is the reaction coefficient which determines the time-scale of the reaction, the second parameter  $\mu_2 \in (0, 1)$  determines the unstable equilibrium, and  $t_S(\boldsymbol{\mu})$  denotes the shock formation time.

We let the initial condition  $u_0(x)$  be a sine-slope decreasing from 1 to 0,

$$(7.4) \quad u_0(x) = \begin{cases} 1 & \text{if } x < -2, \\ \frac{1}{2} - \frac{1}{2} \sin\left(\frac{\pi}{4}x\right) & \text{if } -2 \leq x \leq 2, \\ 0 & \text{if } x > 2. \end{cases}$$

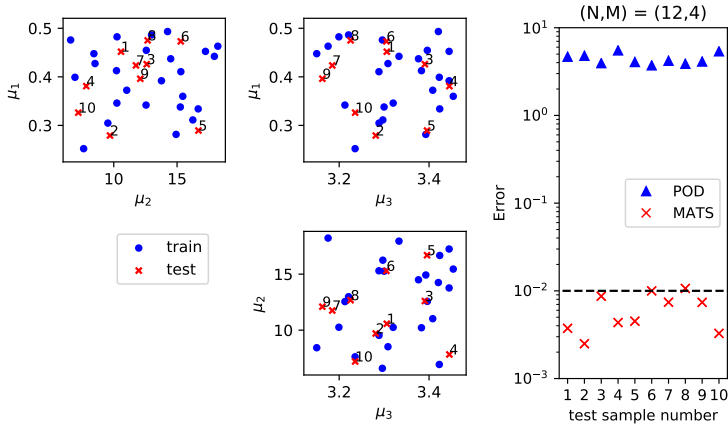


FIG. 7.2. Training and test parameter samples used for the color equation example (left), and  $L^1$ -relative error of the reduced model of dimensions  $(N, M) = (12, 4)$  averaged over time, and corresponding error for POD with dimension  $N$  (right).

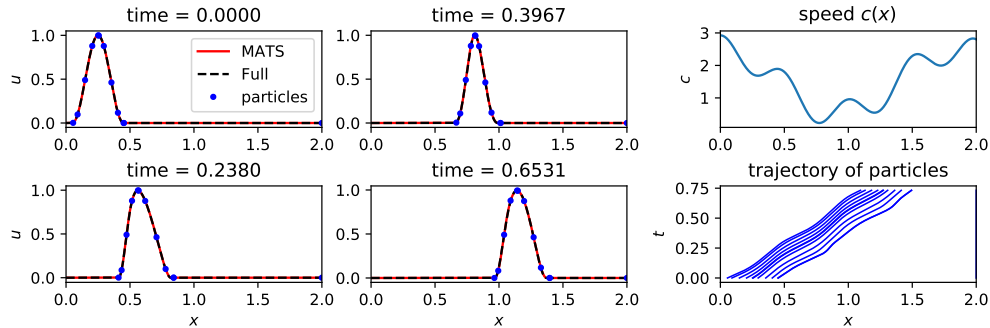


FIG. 7.3. Solution plot for the color equation example (7.1). The reduced-model solution  $\hat{u}$ , full-model solution  $u_\delta$  and speed  $c(x; \mu)$  for the test parameter values  $\mu_1 = 0.43$ ,  $\mu_2 = 12.60$ ,  $\mu_3 = 3.39$  corresponding to test parameter number 3 in Figure 7.2. The dimensions of this reduced model is  $(N, M) = (12, 4)$ .

For the full model, small mesh-size is necessary due to the time-step restriction  $\mu_1 \Delta t \ll 1$  (see [11]). Moreover, since the spatial and temporal resolutions are related by the ratio  $\lambda = \Delta t / \Delta x$  away from zero, small grid-size is required when the parameter  $\mu_1$  is large.

The strategy for collecting training samples is the same as in the previous example: We run the full model for various parameter values, then collect solutions which belong to a local time window close to the initial time, and these early solutions form the local snapshots  $\mathcal{S}_l$ . Then we widen the time interval and collect solutions for the global snapshots  $\mathcal{S}_g$ .

For this example, we perform *two* experiments. In the individual experiments, the coefficient  $\mu_1$  will be set to relatively lower and higher range corresponding to slow and fast reaction regimes. We distinguish the two ranges of parameters by the superscripts S and F. The parameters will be in the respective parameter domains,

$$(7.5) \quad \mathcal{D}^S := [50, 60] \times [0.1, 0.9], \quad \mathcal{D}^F := [100, 150] \times [0.1, 0.9].$$

The parameters for the snapshots are 25 samples drawn from uniformly distributed random samples in their respective domains  $\mathcal{D}^S, \mathcal{D}^F$ ; we denote the set of these samples to be  $\mathcal{N}_1^S, \mathcal{N}_1^F$ . Since the reaction rate  $\mu_1$  controls the time-scale, we collect the full-model solution during equally spaced times near the initial time  $t = 0$  scaled by this rate,

$$(7.6) \quad \mathcal{T}_1^S(\boldsymbol{\mu}) := \left\{ \frac{0.1}{\mu_1} i : i = 0, 1, \dots, 4 \right\}, \quad \mathcal{T}_1^F(\boldsymbol{\mu}) := \left\{ \frac{0.01}{\mu_1} i : i = 0, 1, \dots, 4 \right\}.$$

The local snapshots are taken at the time-parameter values,

$$(7.7) \quad \mathcal{H}_1^S := \{(t, \boldsymbol{\mu}) : t \in \mathcal{T}_1^S(\boldsymbol{\mu}), \boldsymbol{\mu} \in \mathcal{N}_1^S\}, \quad \mathcal{H}_1^F := \{(t, \boldsymbol{\mu}) : t \in \mathcal{T}_1^F(\boldsymbol{\mu}), \boldsymbol{\mu} \in \mathcal{N}_1^F\},$$

so we obtain  $|\mathcal{S}_1^S| = |\mathcal{S}_1^F| = 125$  local snapshots.

Global snapshots  $\mathcal{S}_g^S, \mathcal{S}_g^F$  (4.5) are taken over a longer time-interval,

$$(7.8) \quad \begin{aligned} \mathcal{H}_g^S &:= \mathcal{H}_1^S \cup \{(t, \boldsymbol{\mu}) : t \in \mathcal{T}_g^S(\boldsymbol{\mu}), \boldsymbol{\mu} \in \mathcal{N}_1^S\}, \\ \mathcal{H}_g^F &:= \mathcal{H}_1^F \cup \{(t, \boldsymbol{\mu}) : t \in \mathcal{T}_g^F(\boldsymbol{\mu}), \boldsymbol{\mu} \in \mathcal{N}_1^F\}, \end{aligned}$$

in which

$$(7.9) \quad \begin{aligned} \mathcal{T}_g^S(\boldsymbol{\mu}) &:= \left\{ \frac{0.5 + 1.95i}{\mu_1} : i = 0, \dots, 9 \right\}, \\ \mathcal{T}_g^F(\boldsymbol{\mu}) &:= \left\{ \frac{0.05 + 5.55i}{\mu_1} : i = 0, \dots, 9 \right\}. \end{aligned}$$

So for each experiment  $|\mathcal{S}_g^S| = |\mathcal{S}_g^F| = 375$  snapshots are collected.

The online reduced model is run up to the time-steps

$$(7.10) \quad K^S := 200, \quad K^F(\boldsymbol{\mu}) := \left\lfloor \frac{1}{\Delta t} \left( \frac{10.0}{\mu_1} \right) \right\rfloor.$$

For the slow case, we set a fixed number of time-steps  $K^S$  well before the shock forms, whereas for the fast case, we time-step up to the shock formation. We do not expect the method to perform well close to the shock formation time in the fast case, so we set a stopping criteria: If the particles become too close or if the ordering of the particles change before  $K^F(\boldsymbol{\mu})$  is reached, we discard the result (see [Figure 7.4](#)).

Runtime speedup behavior is very similar to the previous example [subsection 7.1](#), see [Figure 7.1](#). The average  $L^1$  relative error over different 10 different test values, for various dimensions of  $(N, M)$  in our approximation (3.9) is shown in [Figure 7.4](#). Although the problem is nonlinear, the error behavior for the slow reaction case is similar to that of the linear example ([Figure 7.1](#)). In contrast, for the fast reaction case, one observes an erratic behavior in the error with respect to the dimensions, and note that there are combinations of  $(N, M)$  that do not reach the shock formation time due to the loss of monotonicity in the particles. However, the method does provide an approximation at the relative error level of  $10^{-3}$  for certain choices of  $(N, M)$  near the diagonal ( $N = M$ ). As in the previous example, this indicates that the  $(N, M)$ -width for this problem is also small, a numerical verification that the solution has a small  $(N, M)$ -width, despite the nonlinearity in both the flux and the source terms.

A plot of the reduced-model and the full-model solution for the fast reaction case is shown in [Figure 7.5](#).

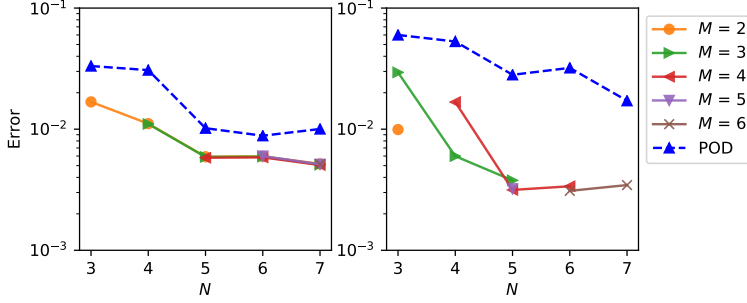


FIG. 7.4. Average relative error plot for the reactive Burgers' equation example (7.3) for various dimensions  $(N, M)$  for the slow reaction case (left) and the fast reaction case (right).

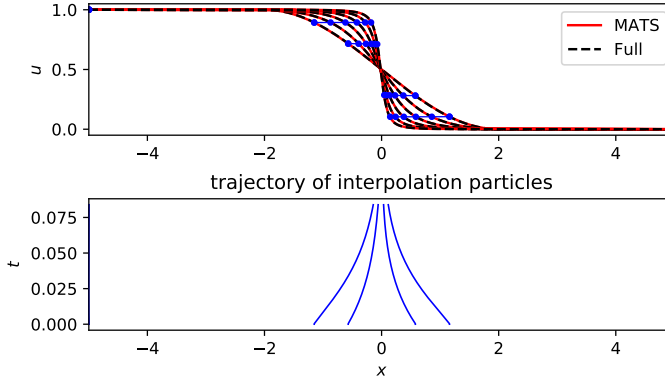


FIG. 7.5. Solution plot for the Burgers equation example (7.3). The reduced-model solution  $\hat{u}$  versus the full-model solution  $u_\delta$  for the test parameter values  $\mu_1 = 118.26$ ,  $\mu_2 = 0.5240$ . The dimensions of this reduced model is  $(N, M) = (5, 4)$ , and the solutions are shown at the times  $t = 0.0000, 0.0152, 0.0305, 0.0458, 0.0610, 0.0763$ .

**7.3. Discussion.** We make some remarks regarding the behavior of the error and shock formation for the Burgers' example.

The error shown for both examples shown in Figures 7.1 and 7.4 do not exhibit monotone decrease with respect to  $N$  and  $M$ . Moreover, the accuracy does not appear to approach the levels of error for the full model. Similar behavior is also observed in the numerical examples of recent related works [17]. The likely contributing factors are (1) the low-rank Lagrangian frame causes the corresponding 1D mesh to be irregular, and the subspace  $\mathbb{V}_{\text{rb}}(t, \boldsymbol{\mu})$  to be non-conformal with respect to the full-model discretization  $\mathbb{V}_\delta$ , (2) the first-order time-update with uniform time-step-size  $\Delta t$  we employed in subsection 5.3 is a naïve projection of the first order full-model time-update which could yield less-than-optimal updates considering the projection to  $\mathbb{V}_{\text{rb}}(t, \boldsymbol{\mu})$ , (3) the approximation error from the change of basis can accumulate over time, (4) better snapshot collection may be necessary for improved construction of  $\mathbb{V}_{\text{rb}}$  and  $\mathbb{T}_{\text{rb}}$ .

In the Burgers' example shocks form, which implies that the characteristic curves merge. Such singular behavior in the characteristic curves is problematic for the current formulation of the reduced model. For example, in the update formula (5.23)

the particles can switch their relative positions during time-stepping. This is a fairly standard phenomena for Lagrangian methods applied to the problem (2.1), but the case for particles  $\{x_i^{(k)}\}_{i=1}^N$  has not yet been studied, to the best of our knowledge. Note that for approximations suggested in [23, 24] using DIP, monotonicity is preserved by construction and the merging characteristics are represented, allowing shock propagation for the reduced model.

**8. Conclusion.** Traditional model reduction methods based on linear approximations are typically ineffective for systems governed by hyperbolic conservation laws because the corresponding solution manifolds exhibit nonlinear transport structures. The proposed approach MATS constructs nonlinear reduced models by transporting subspaces along characteristic curves, which led to speedups of orders of magnitude compared to traditional reduced models and full models in the presented numerical examples. This work highlighted two aspects of this nonlinear reduction approach. First, the Kolmogorov  $(N, M)$ -width was introduced, establishing a notion of best approximation of MATS from the approximation theory point of view. Second, a computational procedure that constructs reduced models based on MATS for physical systems governed by scalar conservation laws was introduced. A crucial feature of the procedure is that the governing equations of the conservation laws are time-stepped in the online phase in contrast to, e.g., data-fit reduced models. Thus the proposed reduced models are explicitly based on the physics (governing equations) of the systems of interest, rather than being predictive in only a data-driven sense.

**Acknowledgments.** The work of the first author (Rim) and second author (Pehrestorfer) was partially supported by the Air Force Center of Excellence on Multi-Fidelity Modeling of Rocket Combustor Dynamics under Award Number FA9550-17-1-0195 and AFOSR MURI on multi-information sources of multi-physics systems under Award Number FA9550-15-1-0038 (Program Manager Dr. Fariba Fahroo). The third author (Mandli) was partially supported by the NSF under Grant No. OAC-1735609 and DMS-1720288.

#### REFERENCES

- [1] R. ABGRALL, D. AMSALLEM, AND R. CRISOVAN, *Robust model reduction by  $L^1$ -norm minimization and approximation via dictionaries: Application to linear and nonlinear hyperbolic problems*, Advanced Modeling and Simulation in Engineering Sciences, 3 (2016), p. 1.
- [2] M. BARRAULT, Y. MADAY, N. C. NGUYEN, AND A. T. PATERA, *An ‘empirical interpolation’ method: application to efficient reduced-basis discretization of partial differential equations*, Comptes Rendus Mathematique, 339 (2004), pp. 667 – 672.
- [3] F. BOLLEY, Y. BRENIER, AND G. LOEPER, *Contractive metrics for scalar conservation laws*, Journal of Hyperbolic Differential Equations, 02 (2005), pp. 91–107.
- [4] K. CARLBERG, *Adaptive  $h$ -refinement for reduced-order models*, International Journal for Numerical Methods in Engineering, 102 (2015), pp. 1192–1210.
- [5] S. CHATURANTABUT AND D. C. SORENSEN, *Nonlinear model reduction via discrete empirical interpolation*, SIAM Journal on Scientific Computing, 32 (2010), pp. 2737–2764.
- [6] C. GREIF AND K. URBAN, *Decay of the Kolmogorov  $N$ -width for wave problems*, Applied Mathematics Letters, 96 (2019), pp. 216 – 222.
- [7] J. S. HESTHAVEN, G. ROZZA, AND B. STAMM, *Certified Reduced Basis Methods for Parametrized Partial Differential Equations*, Springer Cham, Cham, Switzerland, 2016.
- [8] A. IOLLO AND D. LOMBARDI, *Advection modes by optimal mass transfer*, Phys. Rev. E, 89 (2014), p. 022923.
- [9] P. D. LAX, *Hyperbolic Systems of Conservation Laws and the Mathematical Theory of Shock Waves*, Society for Industrial and Applied Mathematics, 1973.
- [10] K. LEE AND K. T. CARLBERG, *Model reduction of dynamical systems on nonlinear manifolds using deep convolutional autoencoders*, Journal of Computational Physics, 404 (2020),

- p. 108973.
- [11] R. LEVEQUE AND H. YEE, *A study of numerical methods for hyperbolic conservation laws with stiff source terms*, Journal of Computational Physics, 86 (1990), pp. 187 – 210.
  - [12] R. J. LEVEQUE, *Finite Volume Methods for Hyperbolic Problems*, Cambridge University Press, Cambridge, 1st ed., 2002.
  - [13] M. NONINO, F. BALLARIN, G. ROZZA, AND Y. MADAY, *Overcoming slowly decaying Kolmogorov  $n$ -width by transport maps: application to model order reduction of fluid dynamics and fluid–structure interaction problems*, Preprint, (2019), [arXiv:1911.06598](https://arxiv.org/abs/1911.06598).
  - [14] M. OHLBERGER AND S. RAVE, *Nonlinear reduced basis approximation of parameterized evolution equations via the method of freezing*, Comptes Rendus Mathématique, 351 (2013), pp. 901 – 906.
  - [15] M. OHLBERGER AND S. RAVE, *Reduced basis methods: Success, limitations and future challenges*, Proceedings of the Conference Algorithmy, (2016), pp. 1–12.
  - [16] S. G. P. BENNER AND K. WILLCOX, *A survey of projection-based model reduction methods for parametric dynamical systems*, SIAM Rev., 57 (2015), pp. 483–531.
  - [17] B. PEHERSTORFER, *Model reduction for transport-dominated problems via online adaptive bases and adaptive sampling*, tech. report, 2018.
  - [18] B. PEHERSTORFER AND K. WILLCOX, *Online adaptive model reduction for nonlinear systems via low-rank updates*, SIAM Journal on Scientific Computing, 37 (2015), pp. A2123–A2150.
  - [19] A. PINKUS,  *$n$ -Widths in Approximation Theory*, Springer, Berlin, Heidelberg, 1985.
  - [20] J. REISS, P. SCHULZE, J. SESTERHENN, AND V. MEHRMANN, *The shifted proper orthogonal decomposition: A mode decomposition for multiple transport phenomena*, SIAM Journal on Scientific Computing, 40 (2018), pp. A1322–A1344.
  - [21] D. RIM, *Dimensional splitting of hyperbolic partial differential equations using the Radon transform*, SIAM Journal on Scientific Computing, 40 (2018), pp. A4184–A4207.
  - [22] D. RIM AND K. MANDLI, *Displacement interpolation using monotone rearrangement*, SIAM/ASA Journal on Uncertainty Quantification, 6 (2018), pp. 1503–1531.
  - [23] D. RIM AND K. T. MANDLI, *Model reduction of a parametrized scalar hyperbolic conservation law using displacement interpolation*, Preprint, (2018), [arXiv:1805.05938](https://arxiv.org/abs/1805.05938).
  - [24] D. RIM, K. T. MANDLI, AND K. URBAN, *Displacement interpolation by pieces (DIP): Nonlinear interpolation for model reduction of nonlinear conservation laws*, In Preparation, (2019).
  - [25] D. RIM, S. MOE, AND R. LEVEQUE, *Transport reversal for model reduction of hyperbolic partial differential equations*, SIAM/ASA Journal on Uncertainty Quantification, 6 (2018), pp. 118–150.
  - [26] C. W. ROWLEY AND J. E. MARSDEN, *Reconstruction equations and the Karhunen-Loève expansion for systems with symmetry*, Physica D, (2000), pp. 1–19.
  - [27] D. SERRE, *Systems of Conservation Laws 1: Hyperbolicity, Entropies, Shock Waves*, Cambridge University Press, 1999.
  - [28] J. SESTERHENN AND A. SHAHIRPOUR, *A characteristic dynamic mode decomposition*, Theoretical and Computational Fluid Dynamics, 33 (2019), pp. 281–305.
  - [29] T. TADDEI, *A registration method for model order reduction: data compression and geometry reduction*, Preprint, (2019), [arXiv:1906.11008](https://arxiv.org/abs/1906.11008).
  - [30] T. TADDEI, S. PEROTTO, AND A. QUARTERONI, *Reduced basis techniques for nonlinear conservation laws*, ESAIM: M2AN, 49 (2015), pp. 787–814.
  - [31] V. N. TEMLYAKOV, *Nonlinear Kolmogorov widths*, Mathematical Notes, 63 (1998), pp. 1573 – 8876.
  - [32] L. N. TREFETHEN, *Approximation Theory and Approximation Practice*, Society for Industrial and Applied Mathematics, Philadelphia, PA, USA, 2012.
  - [33] O. M. F.-X. V. V. EHRLACHER, D. LOMBARDI, *Nonlinear model reduction on metric spaces. application to one-dimensional conservative PDEs in Wasserstein spaces*, Preprint, (2019), [arXiv:1909.06626](https://arxiv.org/abs/1909.06626).
  - [34] C. VILLANI, *Topics in Optimal Transportation*, American Mathematical Society, Providence, RI, 2003.
  - [35] C. VILLANI, *Optimal Transport: Old and New*, vol. 338, Springer Science & Business Media, 2008.
  - [36] G. WELPER, *Interpolation of functions with parameter dependent jumps by transformed snapshots*, SIAM Journal on Scientific Computing, 39 (2017), pp. A1225–A1250.
  - [37] G. WELPER, *Transformed snapshot interpolation with high resolution transforms*, Preprint, (2019), [arXiv:1901.01322](https://arxiv.org/abs/1901.01322).
  - [38] M. YANO, A. T. PATERA, AND K. URBAN, *A space-time hp-interpolation-based certified reduced basis method for Burgers’ equation*, Mathematical Models and Methods in Applied Sciences, 24 (2014), pp. 1903–1935.